

Review

Review on the Test Methods and Devices for Mechanical Properties of Hydrate-Bearing Sediments

Mingtao Chen^{1,2,3}, Yanlong Li^{2,3,*} , Şükrü Meray⁴ , Nengyou Wu^{1,2,3,*} , Qiaobo Hu^{2,3}, Yajuan Zhang^{1,2,3}, Lin Dong^{2,3}, Guigang Yu^{2,5} and Haiyang Jiang^{2,3}

- ¹ College of Oceanography, Hohai University, Nanjing 210098, China; liyanlong@mail.cgs.gov.cn (M.C.); dddzhang@qnlm.ac (Y.Z.)
 - ² Laboratory for Marine Mineral Resources, Qingdao National Laboratory for Marine Science and Technology, Qingdao 266237, China; juguoshuai@nepu.edu.cn (Q.H.); marine_oil@qnlm.ac (L.D.); wzhan@qnlm.ac (G.Y.); qlin@qnlm.ac (H.J.)
 - ³ Key Laboratory of Gas Hydrate, Ministry of Natural Resources, Qingdao Institute of Marine Geology, Qingdao 266237, China
 - ⁴ Department of Petroleum and Natural Gas Engineering, Batman University, Batman 72060, Turkey; sukru.meray@batman.edu.tr
 - ⁵ Faculty of Engineering, China University of Geosciences, Wuhan 430074, China
- * Correspondence: ylli@qnlm.ac (Y.L.); wunyu@ms.giec.ac.cn (N.W.)

Abstract: Commercial exploitation of marine natural gas hydrate (NGH) is crucial for energy decarbonization. However, hydrate production would weaken reservoir mechanical properties and trigger geohazards. Experimental instruments are the basis to obtain the mechanical responses of hydrate-bearing sediments (HBS). Considering the reservoir deformation processes from elastic deformation to residual deformation during hydrate exploitation, this study comprehensively reviewed the feasibility and mechanical research progress of the bender element, resonance column, atomic force microscope, triaxial shear, direct shear, ring shear, and static penetration in mechanical testing. Each test method's precision and sample size were comprehensively compared and analyzed. Finally, the limitations and challenges of the current mechanical testing methods for HBS were discussed, and their future development directions were proposed. The proposed development direction in mechanical testing methods is expected to provide insightful guidance for the development of instruments and improve the understanding of the mechanical behavior of HBS.

Keywords: natural gas hydrate; mechanical testing methods; hydrate-bearing sediments; mechanical behaviors; hydrate exploitation



Citation: Chen, M.; Li, Y.; Meray, Ş.; Wu, N.; Hu, Q.; Zhang, Y.; Dong, L.; Yu, G.; Jiang, H. Review on the Test Methods and Devices for Mechanical Properties of Hydrate-Bearing Sediments. *Sustainability* **2022**, *14*, 6239. <https://doi.org/10.3390/su14106239>

Academic Editor: Andrea Nicolini

Received: 19 April 2022

Accepted: 11 May 2022

Published: 20 May 2022

Publisher's Note: MDPI stays neutral with regard to jurisdictional claims in published maps and institutional affiliations.



Copyright: © 2022 by the authors. Licensee MDPI, Basel, Switzerland. This article is an open access article distributed under the terms and conditions of the Creative Commons Attribution (CC BY) license (<https://creativecommons.org/licenses/by/4.0/>).

1. Introduction

Natural gas hydrate (NGH), is an ice-like crystalline substance, distributed widely in deep marine deposits and the permafrost with substantial reserves [1–3]. Total methane storage worldwide in NGH amounts to approximately $2 \times 10^{16} \text{ m}^3$ [4]. Global energy consumption is facing adjustments because of increasing global warming and frequent extreme weather events, especially the need for peak carbon dioxide emissions and carbon neutrality. NGH has become one of the most promising alternative energy resources for global economic development because of its low-carbon characteristic [5,6]. It is greatly expected to be sufficiently explored and economically exploited by the late 2030s.

Gas production from NGH involves the heat transformation and change in the internal skeleton structure in HBS [7], leading to changes in the cementing and rolling sliding of particles [8,9]. Dissociation of hydrates leads to a decrease in effective stress due to the release of methane gas and water [10], triggering the risk of geohazards such as seabed subsidence, wellbore failure, and large-scale submarine landslide collapse [11–15]. Furthermore, the safety of drilling platforms is seriously affected by the creep of the

reservoir [16–18]. Therefore, the mechanical properties obtained from the reservoir are of great importance in forecasting the potential risk of geological hazards [19].

Mechanical testing devices are tools that significantly assist in the mechanical-behavior research of HBS, they directly determine the accuracy of the basic mechanical properties of HBS, and significantly affect the understanding of geological-disaster risk [20,21]. Through analyzing the stress–strain curve, mechanical parameters (such as peak strength, cohesion, friction angle, etc.) can be obtained [22–25]. Considering the deformation characteristic of a hydrate reservoir in different deformation stages, the deformation progress stages can be divided into the elastic section, elastic-plastic section, and residual section [6,26]. For testing the above deformation section, many devices have been constructed. The bender elements and resonance column test devices have been used to test the elastic deformation in hydrate reservoirs [27,28]. In addition, the triaxial and direct shear test techniques are mainly used in measuring the elastic-plastic deformation behavior of HBS [29,30]. For analyzing the mechanical parameters of HBS in a large deformation, ring shear has been widely used to test residual deformation [31].

Many scholars have studied the mechanical behavior of HBS [29,32,33]. However, there is still a lack of a comprehensive review of experimental devices in testing the mechanical behavior of NGH, and the precision and feasibility of every device is unclear, a situation that is not beneficial for the improvement of existing testing methods and forecasting future development trends.

Therefore, based on a comprehensive review of previous research on the mechanical behavior of HBS, this study compared and analyzed the laboratory mechanical testing devices and their measured results. The limitations of the current hydrate mechanical tests were also investigated. Through analysis of the challenges faced in the current hydrate mechanical tests, the main research points in the future of the mechanical properties of HBS were discussed.

2. Current Progress on HBS Mechanical Testing Methods

Experimental instruments are significant in studying the mechanical behavior of HBS. During the hydrate production process, the reservoir experiences different deformation stages, requiring varying mechanical testing equipment to measure these deformation behaviors. Therefore, this part mainly focuses on summarizing current testing devices in the mechanical testing of HBS and discusses significant progress and limitations.

2.1. Mechanical Properties Characterization Techniques of HBS under Small Strain

2.1.1. Bender Elements Testing Method

Currently, triaxial testing still has some limitations in capturing small-strain features and depicting the small-strain shear modulus of HBS. Although the small-strain shear modulus of a sample can be obtained by setting a local deformation sensor in a triaxial shear, it is still costly and complicated in operation. In contrast, bender elements have been widely used in HBS small-strain tests because of their simple structure and principle [34,35].

The bender elements are made of a transmitting bender element and a receiving bending element, and the sample is loaded by energized vibration (Figure 1). When a certain frequency of excitation signal voltage pulse is applied, the shear wave perpendicular to the vibration direction, which is generated by the transmitting bender element, is transmitted to the receiving bender element [36,37]. The entire shear-wave transmission time can be obtained by amplifying the signal with an external oscilloscope; the shear wave velocity can be calculated by adding the entire shear wave transmission time and sample length [38].

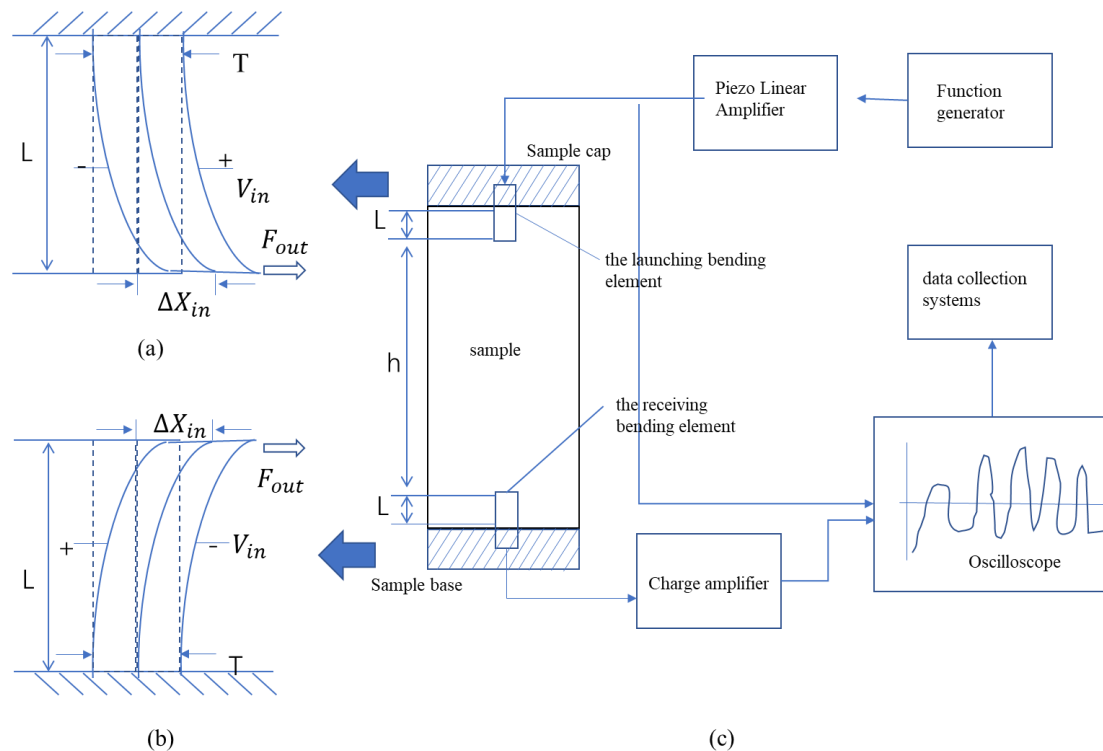


Figure 1. The bender elements test system, modified from [37,39]; (a) working principle of the launching bending element; (b) working principle of the receiving bending element; (c) bending element shear wave velocity test system.

The bender elements were used to test the response mechanism between hydrate saturation and wave velocity to represent the small-strain characteristics of HBS (Figure 2). Considering the response mechanism between wave velocity and hydrate saturation, Hu et al. (2012) found that the hydrate saturation of unconsolidated HBS has a significant effect on compression-wave velocity and shear-wave velocity [38]. A further study of HBS in the South China Sea indicated that the sonic signal was weaker when the hydrate saturation was less than 14% [40]. During the hydrate formation, the compression-wave velocity and the shear-wave velocity increased with increasing saturation. Especially, when the saturation was larger than 14%, the shear-wave velocity showed a sharp increase.

Limited by higher pressure and lower temperature conditions in synthesized NGH, tetrahydrofuran (THF) hydrate and CO₂ hydrate, which are easily synthesized in relatively low temperature and pressure conditions, were used to calculate the mechanical mechanism under micro-seismic loading. Ji et al. (2019) used THF to verify whether the shear-wave velocity can be used to characterize the formation and dissociation of a hydrate [41]. Kim et al. (2013) studied the effect of CO₂-hydrate formation on vibration-wave velocity and found that, when saturation was 0~60%, the compression-wave velocity and shear-wave velocity increased with increasing hydrate saturation [42].

In summary, bender elements are a micro-seismic mechanical testing instrument in the test of the compression-wave velocity and shear-wave velocity of HBS. Different compression-wave velocities and shear-wave velocities can be obtained by different seismic frequencies, but generally in the range of 1–1000 kHz. The current study mainly concentrates on the effect of hydrate saturation and has not paid much attention to the heterogeneous effect. Furthermore, because most bender elements lack axial pressure design, they cannot simulate the elastic mechanical behavior of HBS at a certain depth on the seafloor. Therefore, the impact of axial pressure and integrated CT scanning should be considered to test the heterogeneous characteristics of the sample, making unity in macro and micromechanical testing.

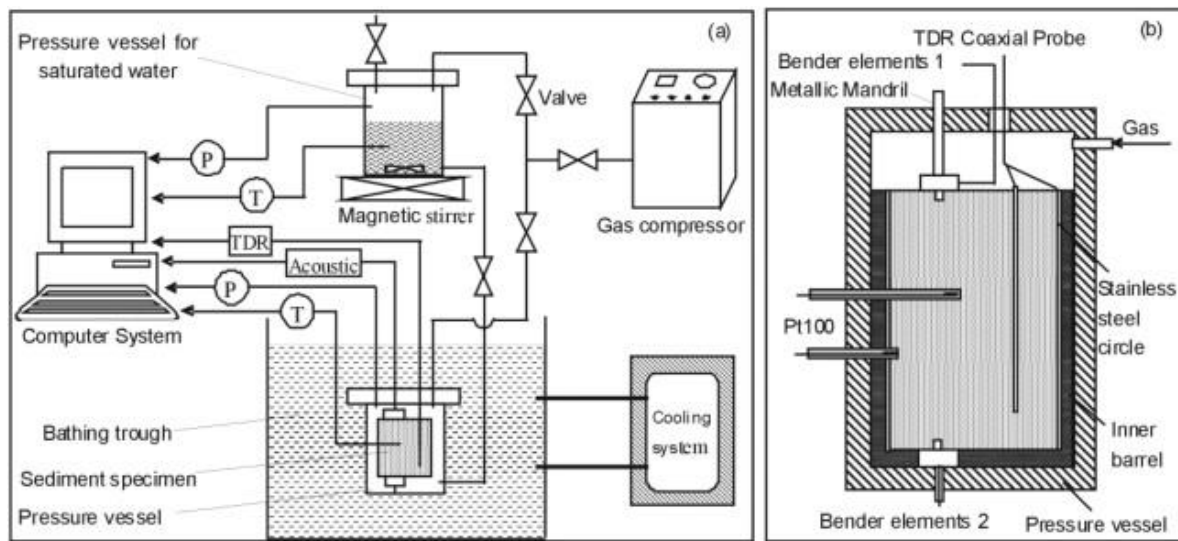


Figure 2. Diagram of bending-element-test system [38]; (a) overall arrangement of bending-element-test system; (b) layout diagram of bending element.

2.1.2. Resonance Column Testing Method

The resonance column is an elastic mechanical test instrument that uses the principle of resonance to apply torsional vibration to a cylindrical soil or rock sample to test the shear-wave velocity [43,44]. It uses the vibration theory of linear viscoelastic cylindrical rods to quantify the velocity of shear waves (Figure 3). The Stokoe resonance column test device can only be used for torsional excitation, but it can also be used for bending excitation by adjustment [45,46]. The modified resonance column can test shear and longitudinal stiffness [47]. According to vibration frequency, voltage, etc., the dynamic shear modulus and damping ratio of the sample can be obtained [48,49].

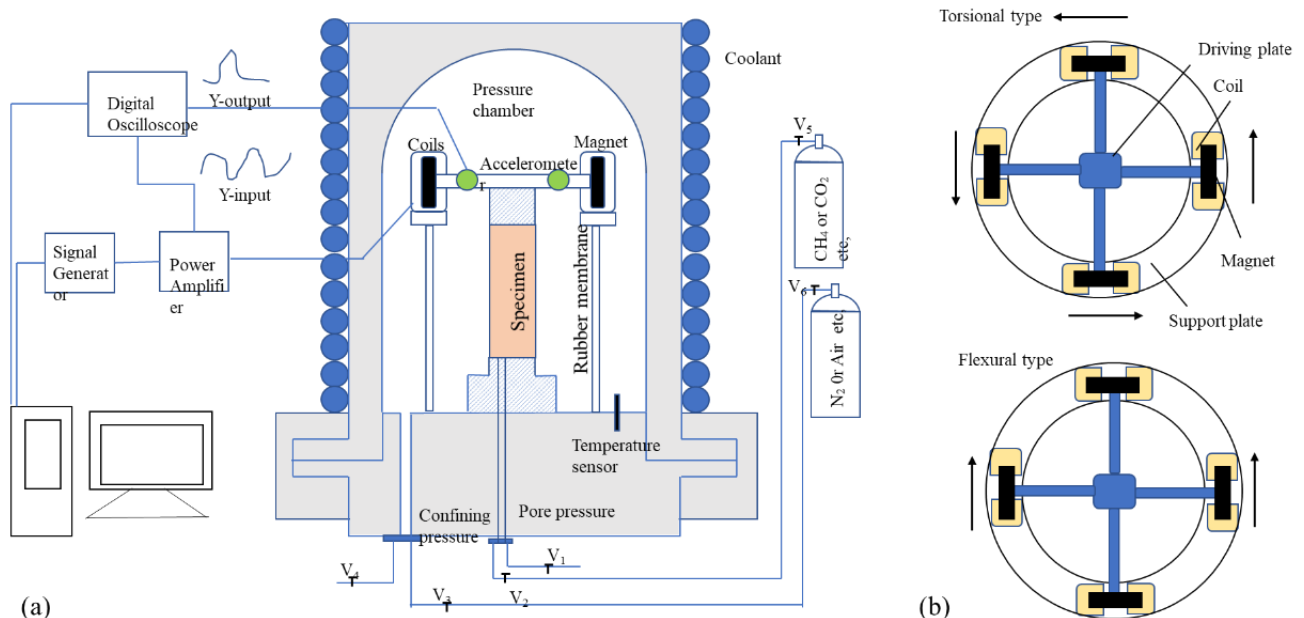


Figure 3. Principle of resonance (Reprinted with permission from Ref. [50]. 1 December 2020, Elsevier); (a) overall arrangement of resonance; (b) excitation system and driving types.

The response mechanism of wave velocity in the mechanical behavior of HBS was studied by comprehensively considering the factors of hydrate saturation, hydrate distribution, and morphology in the resonance column test [51,52], as shown in Table 1. The sample

deformation was considered to be elastic deformation without failure because the strain in the resonance column test was small ($<10^{-4}$).

The existence and distribution of methane hydrate significantly affect the mechanical properties of HBS. Compression- and shear-wave attenuation in dry samples were sensitive to hydrate saturation, verified by unexpected peaks between 3% and 5% saturation [53]. In the core sample, small strain stiffness increased with increasing particle size, hydrate saturation, and effective confining pressure. Furthermore, hydrate-bearing silt sediments with high hydrate saturation had the highest stiffness, up to five times that of non-hydrated silt sediments [54]. The wave velocity obtained in the resonance column test can also be used in evaluating the formation and decomposition of dispersed methane hydrate [52]. The results showed that the relationship between wave speed and hydrate saturation was nonlinear, and there were significant differences during hydrate formation and decomposition. The increase in the damping ratio with an increase in the modulus of HBS can be used to identify the occurrence of hydrates [28].

To make hydrate synthesis simpler, THF hydrate has been used to replace methane hydrate to study the vibrational response of HBS in the resonance column test [55]. Studies showed that the shear modulus increased exponentially with increasing confining pressure, while the damping ratio decreased exponentially under the same conditions [56]. Further study indicated that wave-velocity evolution was generally independent of stress when the hydrate saturation reaches a critical saturation [50].

Table 1. Basic parameters of resonance column.

References	Size (mm)	Test Indicators	Vibration Frequency (Hz)	Shear Strain (%)	Important Discovery
Cascante et al. (1998) [47]	$\Phi 71 \times 136$	Shear and longitudinal stiffness	50–200	10^{-6} – 10^{-5}	P and S waves are affected by stress state but are almost insensitive to the stress history.
Clayton et al. (2005) [57]	$\Phi 70 \times 140$	Shear and longitudinal stiffness	NA	10^{-6}	Hydrate bonding has considerably less impact on bulk modulus.
Priest et al. (2005) [58]	$\Phi 70 \times 140$	Compression and shear-wave velocity	17–400	10^{-5}	A dichotomous relationship was exhibited between compressional and shear wave velocities with hydrate saturation.
Best et al. (2013) [59]	$\Phi 70 \times 140$	Compression and shear-wave velocity	50–550	10^{-4}	Hydrate synthesis methods significantly affect the attenuation properties of shear wave velocity and compression wave velocity.
Liu et al. (2020) [50]	$\Phi 70 \times 140$	Compression and shear-wave velocity	146–154	10^{-6} – 10^{-4}	Wave attenuation of tested specimens decreases with increasing effective confining stress and increases with increasing hydrate saturation.

In summary, the resonance column devices were mainly used to study the shear modulus and damping ratio of the reservoir under different hydrate morphologies, saturations, and confining pressures [57]. They provided a reference for predicting the mechanical behavior of the reservoir under seafloor micro-seismic conditions. The height–diameter ratio shown in reports is generally 2:1 and vibration frequency is 17–550 Hz. However, most resonance column devices cannot consider the effect of axial stress, and obtained shear modulus and damping ratios showed a difference with natural reservoirs. Therefore, axial loading would be a type of instrument to be developed in the future.

2.1.3. Other Promising Techniques

Sand production substantially affects the safety of hydrate exploitation [2,60,61]. Unlocking the mechanical mechanism between sand particles and hydrate particles is the key in control sand production. Therefore, a micro-mechanical testing device has been constructed to test the adhesive force between hydrate particles and ice particles, and the friction force between sediments of the South China Sea and the hydrate particles of THF [62].

The core measurement part of this micro-mechanical testing device includes three programmable electric displacement tables and two high-precision force sensors. The electric displacement table is mainly used to control the X, Y, and Z directions in the test process. Its minimum and maximum speed ($\pm 0.5 \mu\text{m}$) are $1 \mu\text{m/s}$ and 10mm/s , respectively. Its maximum motion range is 25mm (Figure 4). The precision of the high-precision force sensor is $\pm 0.01 \text{mN}$, which can monitor real-time tensile and compressive force.

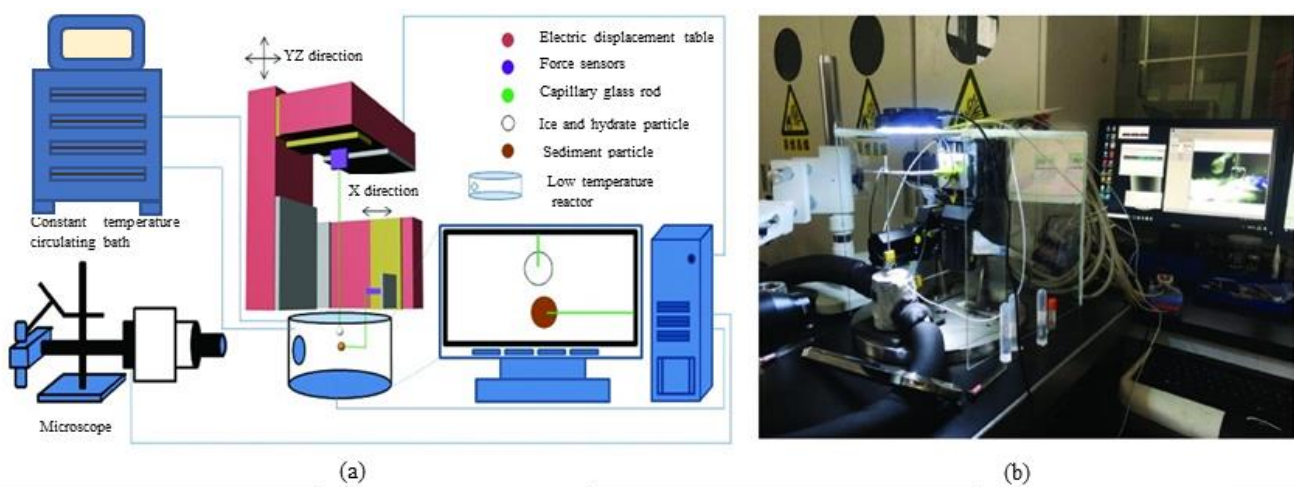


Figure 4. Diagram of the micro-mechanical testing device, modified from [62]; (a) schematic diagram; (b) physical map.

To obtain small-strain mechanical parameters of field sediment samples, Lee et al. (2010) developed a chamber that could measure compression- and shear-wave velocities (Figure 5). Sand, silt, and clay sediments bearing THF hydrates were tested under the vertical effective confining pressure of $0.01\text{--}2 \text{MPa}$. The results demonstrated that the shear-wave and compression-wave velocities were significantly affected by the hydrate saturation, and the small-strain mechanical parameters of hydrate sediments were controlled by the effective stress and the surface of sediments [27].

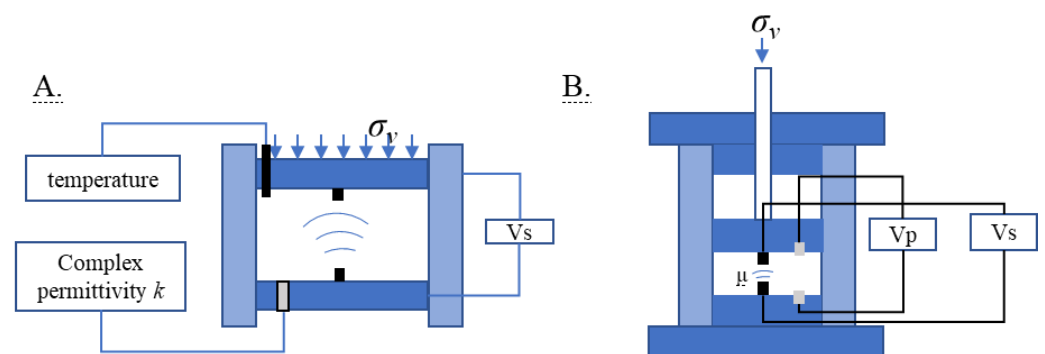


Figure 5. Diagram of chamber in small-strain testing: (A) low fluid-pressure test cell, which can accommodate samples with a height of $4\text{--}5 \text{cm}$ and diameter of 10cm ; (B) high-pressure test cell, designed to test samples with a height of $4\text{--}5 \text{cm}$ and diameter of 6cm [27].

Atomic force microscopy was used mainly in measuring the surface morphology of the material. During the testing process, a nanotip cantilever was used to contact the sample surface, and reflected laser light in the cantilever was used to transmit data of the height change of the probe during the movement to position the receiver to reflect the surface morphology of the sample (Figure 6). In addition to high-resolution imaging functions, atomic force microscopes can also be used in high-precision micromechanical test. In general, the lateral and longitudinal resolution of an atomic force microscope can reach 1 nm and 0.2 nm, respectively.

Atomic force microscopy has been widely used in describing the microscopic morphology of material, the micromechanical properties of rock, and the mechanical characters of biological tissue [63]. The surface morphology of THF hydrates tested by atomic force microscopy showed that the amorphous hydrates more than likely grew at the gas–liquid free interface in lower growth temperatures and smaller grain sizes. The cross-section of the grain interface was V shaped, and its depth and width decreased with the decrease of growth temperature. When polycrystalline hydrates were constrained by the solid–liquid interface, their surface morphology and roughness were regulated by both the growth temperature and contacting solid medium [64].

In summary, atomic force microscopy was mainly used to focus on the observation of the hydrate morphology; however, there are few applications in testing the mechanical behavior of HBS, because of the difficulty in maintaining the high-pressure and low-temperature sample synthesis conditions under the atomic force microscope. Integrating it with nanoindentation [65,66] would be a direction of great importance in observing the process of morphology changes from elastic deformation to the failure of HBS.

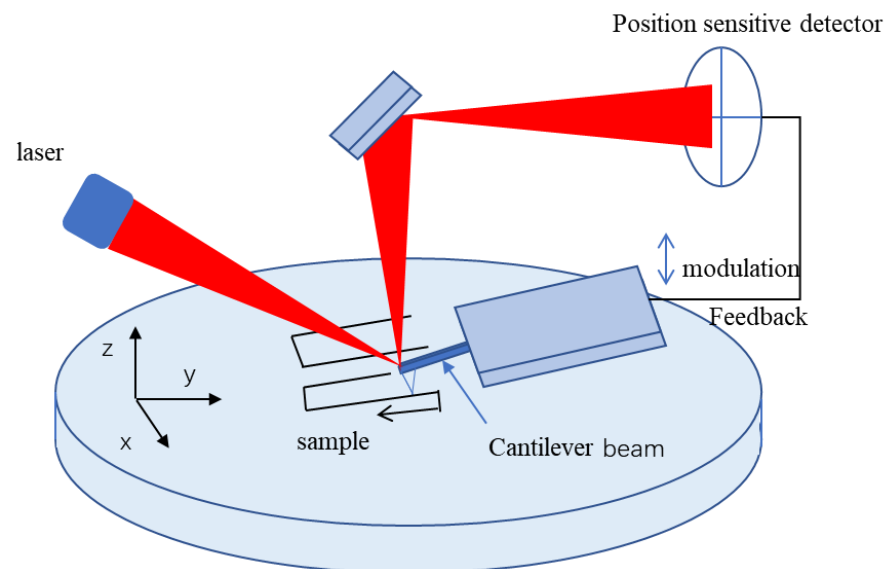


Figure 6. Work principle of atomic force microscopy, modified from [67].

2.2. Current Progress in a Triaxial Shear Test of HBS

2.2.1. Core-Scale Triaxial Shear Devices for HBS

The triaxial device is the most-widely used in testing the macro mechanical properties of HBS (Figure 7). In general, the triaxial test apparatus of HBS was developed based on a conventional geotechnical triaxial shear instrument, adding a gas supply system and temperature control system for hydrate synthetic [23,24,33,68]. In terms of data acquisition, in addition to conventional stress-strain monitoring in the vertical direction and strain-gauged arch monitoring in the lateral direction [69], an acoustic monitoring system was also integrated in the testing of the permeability and porosity of HBS [25,70]. To compare and analyze the triaxial experimental instruments used to test the macroscopic mechan-

ical parameters of hydrate sediments, the basic parameters of the representative triaxial instruments are shown in Table 2.

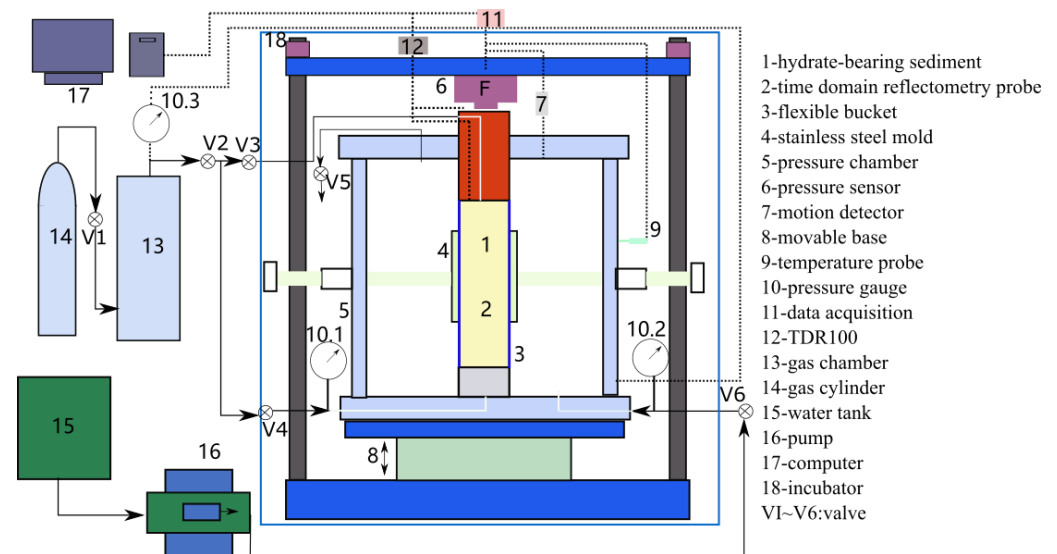


Figure 7. The triaxial test instrument reprinted with permission from Ref. [20]. 1 January 2020, Elsevier.

Previous mechanical research using the triaxial shear experiment focuses mainly on the following: ① Effect of particle type and size on the mechanical behavior of the reservoir. Quartz sand and Toyoura sand are widely used to analyze the mechanical properties of HBS because their mechanical test results are similar to the situ hydrate deposits in the Nankai Trough, Japan [71]. Additionally, because Kaolin is a more easily obtained and synthesized hydrate, it is also widely used by researchers in the synthesizing of hydrates [22,23,68,72]. The particle size distribution is mainly reflected in the difference in the gradation curve, and its influence on the mechanical behavior of the reservoir has also been a subject of interest for some scholars [9,73]. Studies have shown that the sensitivity of silty sand to the effective confining pressure is higher than that of the coarser particles [68]. ② Effect of effective confining pressure on the mechanical behavior of HBS. The maximum strength of HBS increases with increasing effective confining pressure [23,74]. ③ Effect mechanism of hydrate saturation on mechanical behavior. The peak strength of the hydrate reservoirs increases with saturation, as do the cohesion strength and the angle of internal friction [9,75–77]. ④ Effect of different loading ratios on the mechanical parameter of HBS. In the triaxial test, the load control is mainly based on limiting the proportion of the load rate. ⑤ Mechanical behavior of hydrate sediments under drained and undrained shear [78,79]. In the triaxial test, liquids are mainly used to displace the gas in the porosity of the drained shear.

The traditional single stage loading triaxial shear experiment has the disadvantages of requiring repeated samples, complicated sample preparation, and being time-consuming. Therefore, some scholars have developed a multistage loading triaxial shear instrument to measure the small-strain stiffness, permeability, and shear strength of HBS [80,81]. Seol et al. (2014) introduced a multi-parameter characterization chamber for the mechanical testing of HBS [80]. The device has basic functions such as hydrate synthesis, temperature, and pressure monitoring, and can acquire multiple physical parameters from the sample (Figure 8). The sample size is $\Phi 50.8 \times 152.4$ mm, and the maximum confining pressure loading capacity is 20 MPa. Axial loading is achieved by pushing a hydraulic piston rod with the ability to measure volumetric strain. The acoustic impedance of the P-wave crystal is ~ 33.7 MRayl, and the acoustic impedance of the S-wave crystal is ~ 17.9 MRayl. The resonant frequency of the above impedance is 250 kHz.

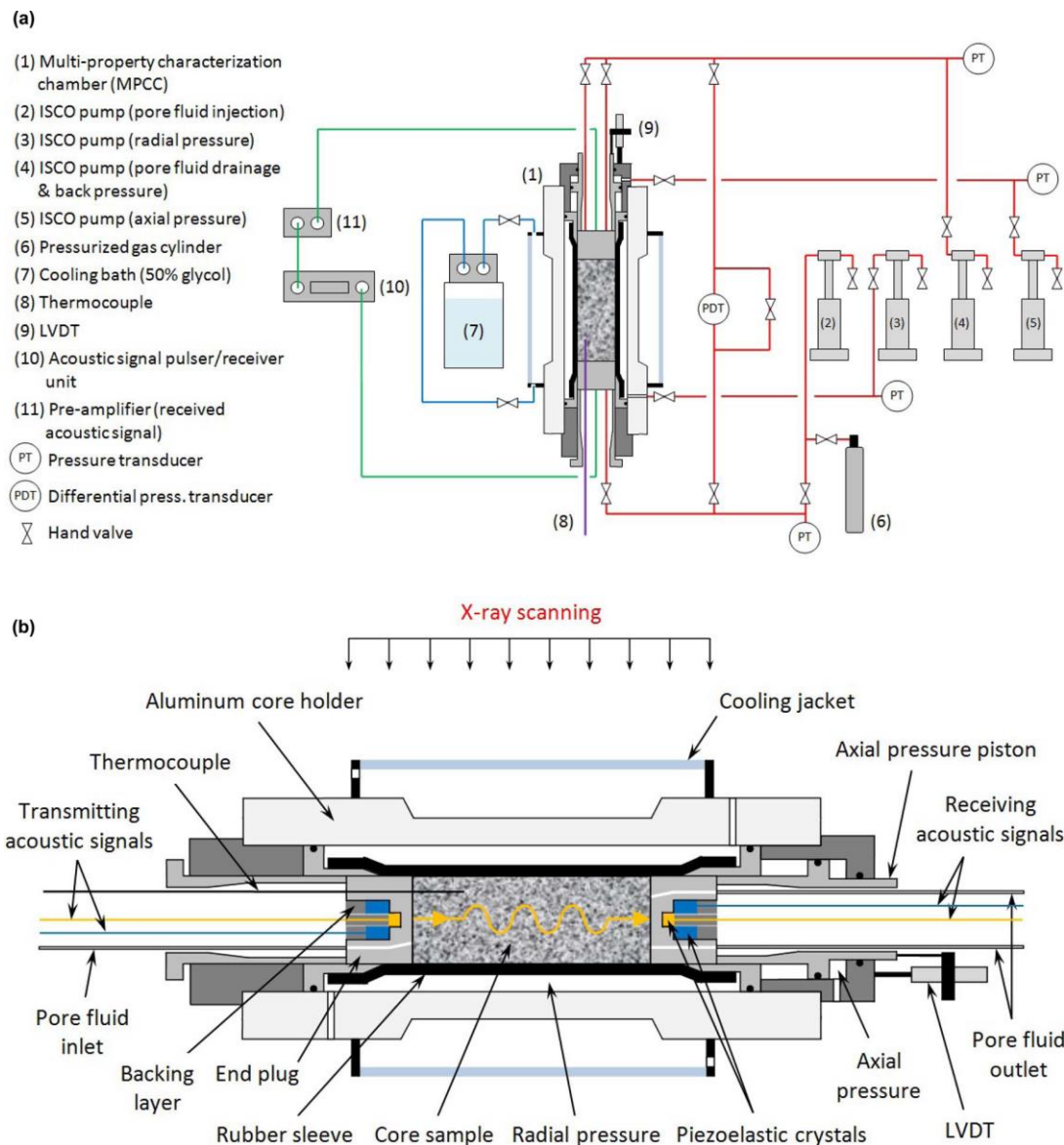


Figure 8. Multi-stage loading triaxial shear instrument (Reprinted with permission from Ref. [80], 2014, Elsevier); (a) overall hydraulic and acoustic flow loop; (b) detailed components of chamber.

Even though triaxial shear has been sufficiently used in researching the mechanical properties of HBS, it still has many limitations:

- (1) No reference standard for sample preparation, hindering the comparison of the mechanical behavior of different triaxial shear experiments. Reported sample sizes are various, and the overall height–diameter ratio is about 2:1. Due to large differences in sample size and experimental conditions between different triaxial shear experiments, the experimental results reported in different kinds of literature cannot be directly compared. It is recommended to standardize the relevant specifications for sample preparation and testing for analysis of different test results.
- (2) The sample preparation size of a specific triaxial shear instrument is fixed, which is not beneficial for the mechanical testing of different height samples in the same instrument. Additionally, it is also inconvenient to determine the scale effect of the sample.
- (3) Coarse-grained sand is mainly used for sample preparation, and less from situ sediments on the seabed. To address the difficulty in synthesizing hydrates from deep-sea

silty sediments, it is recommended to strengthen the research and development of sample-preparation technology.

Table 2. Comparison of basic parameters of the triaxial shear instrument.

Unit Properties	Dalian University of Technology, China	Dalian University of Technology, China	National Institute of Advanced Industrial Science and Technology, Tsukuba, Japan	Yamaguchi University, Japan	Heriot-Watt University, Edinburgh, UK	Institute of Mechanics, Chinese Academy of Sciences, China	Guangzhou Institute of Energy Conversion, Chinese Academy of Sciences, China	Qingdao Institute of Marine Geology, China Geological Survey, China
Type	DDW-600	NA	NA	NA	Tri-Scan 250	NA	NA	TSZ-2
Sample size (mm)	Φ 61.8 × 125	Φ 50 × 100	Φ 50 × 100	Φ 30 × 60	Φ 50 × 100	Φ 39.1 × 80	Φ 50 × 100	Φ 39.1 × 120
Temperature Control range (°C)	−30–25	−20–25	−20–20	−35–50	−20–50	−20–20	−30–50	−20–40
Confining pressure range (MPa)	0–25	0–30	0–20	0–30	0–40	0–14	0–30	0–15
Temperature control pattern	Constant temperature pump + heat exchanger	Constant temperature pump + heat exchanger	Refrigeration tank cooling (Glycol)	Incubator	Constant temperature water bath	Incubator	Constant temperature water bath	Incubator
Temperature control accuracy (°C)	±0.5	±0.5	±0.5	±0.1	NA	±0.5	NA	±0.1
Pressure control accuracy (MPa)	±0.01	±0.01	NA	±0.1	NA	±0.098	0.2%FS	±0.015
External monitoring	NA	NA	NA	NA	NA	NA	NA	Wave monitor
Maximum loading capacity (KN)	600	60	200	200	250	NA	250	50
Volume strain	NA	NA	yes	yes	yes	NA	NA	NA
References	Luo et al. (2016) [72]	Li et al. (2011) [22]	Miyazaki et al. (2011) [23]	Hyodo et al. (2014) [82]	Yang et al. (2019) [83]	Zhang et al. (2010) [84]	Guan et al. (2017) [85]	Dong et al. (2020) [25]

NA: the data is not available.

2.2.2. X-CT Based Triaxial Shear Devices

Computed tomography (CT) is very important in obtaining the microstructure of HBS. In CT testing, according to the different absorption capacities of X or γ rays of each component in HBS, the attenuation coefficient was used in reconstructing the sediment microstructure in 2D or 3D [35,86]. The CT technology, which is applied widely and has a high resolution, can obtain the distribution of each component in HBS without destroying the original samples [26]. Furthermore, the permeability and porosity of HBS can also be obtained [6,86]. Furthermore, the macro and micro comprehensive detection of the mechanical properties of HBS can be realized by integrating it with triaxial test apparatus [87,88], which has important implications for understanding the microscopic dynamic deformation mechanism of hydrate particles [89].

The dynamic morphology of hydrate was the focus of micromechanical research. As the 2D CT-scan image shows, the HBS sample with a size of $\Phi 52.6 \times 120$ mm appears as a stratification phenomenon at different depths [87]. Chen et al. (2018) studied the relative permeability of HBS reservoirs from the pore-scale using an X-ray CT scanner and established the relationship between relative permeability and saturation based on the Boltzmann method [90]. The sample size used in the CT scanner is $\Phi 8.6 \times 39.3$ mm, and

the scanning parameters are 105 KV, 269 1 A, 250 ms exposure, 28.77 μm resolution and no filter. In other research, the porosity distribution and skeleton characteristics of sand particles were also investigated with a sample size of $\Phi 6.35 \times 20 \text{ mm}$ by using a micro-CT scanner [91].

The mechanical mechanism of HBS is another research point. Analysing the micromechanical behavior of the HBS sample with a size of $\Phi 9.5 \times 19 \text{ mm}$, Lei et al. (2020) suggested that the increase in reservoir strength is due to hydrates in skeleton particles; thus, hydrates combined with the sand skeleton to jointly bear the load [92]. A triaxial test based on microfocus X-ray computed tomography can quantitatively analyze the influence of thermal dissociation on the mechanical behavior of hydrate-bearing sandstone [93]. Further studies have shown that in the stress strain linear region of a cemented hydrate, the hydrate-cemented clusters moved while small hydrate particles would aggregate to the periphery of the clusters. [94].

Although CT scanning has advantages in identifying HBS deformation, it still fails to distinguish water and hydrates in voids using grayscale. To distinguish water and hydrates, studies have shown that adding dissolved salts in water is feasible [95,96] or using special guest molecules [97] can distinguish the two phases. However, the asynchrony of the scanning and loading processes makes it difficult to capture the dynamical features of hydrate growth and dissociation. As the resolution affects the test results of microscopic deformation, an improvement in resolution when using CT scanning to observe the microscopic deformation of hydrate-bearing sediments is required.

2.2.3. Triaxial Shear Device for Pressure-Coring Samples

Mechanical properties of gas HBS were substantially obtained by using synthetic methane hydrates, however, its test results contained deviation from natural HBS. The latest coring technology, which can maintain the in-situ hydrology pressure and temperature of reservoirs, allowed to recover natural HBS and to investigate their petrophysical characters for predicting gas production [76,98]. The macro mechanics and micro deformation of HBS can be observed by combining it with triaxial or X-ray CT scanning [99–101].

In the Nankai Trough of Japan and the Shenhu area of the South China Sea, pressure core samples were obtained using in-situ pressure-coring technology (Figure 9). Priest reported a pressure-coring triaxial test instrument with a maximum confining pressure of 25 MPa [54], performing small or large deformations in hydrate core samples with an aspect ratio of 2:1. Under the triaxial mechanical test, the permeability of the sample can be obtained by measuring the fluid that flows through the sample. When calculating the effect of hydrate dissociation, the volume of methane can be quantified using coring technology [102]. To measure the sediment structure, primary-wave velocity (PWV), density, and shear strength under pressurized conditions, Jin et al. (2016) developed a novel X-ray CT-scanning system and an attenuated total reflection infrared probe, which were integrated into an instrumented pressure test chamber in non-destructive pressure core analysis tools [87]. The stiffness and compressive properties of offshore hydrate sediments on the east coast of India were studied by using the effective stress chamber and direct shear chamber (Figure 10) in the pressure core characterization tool [103]. The diameters of the specimens used for the effective stress chamber and the direct shear experiments were $\Phi 50.8 \times 60 \text{ mm}$ and $\Phi 16 \times 60 \text{ mm}$, respectively.

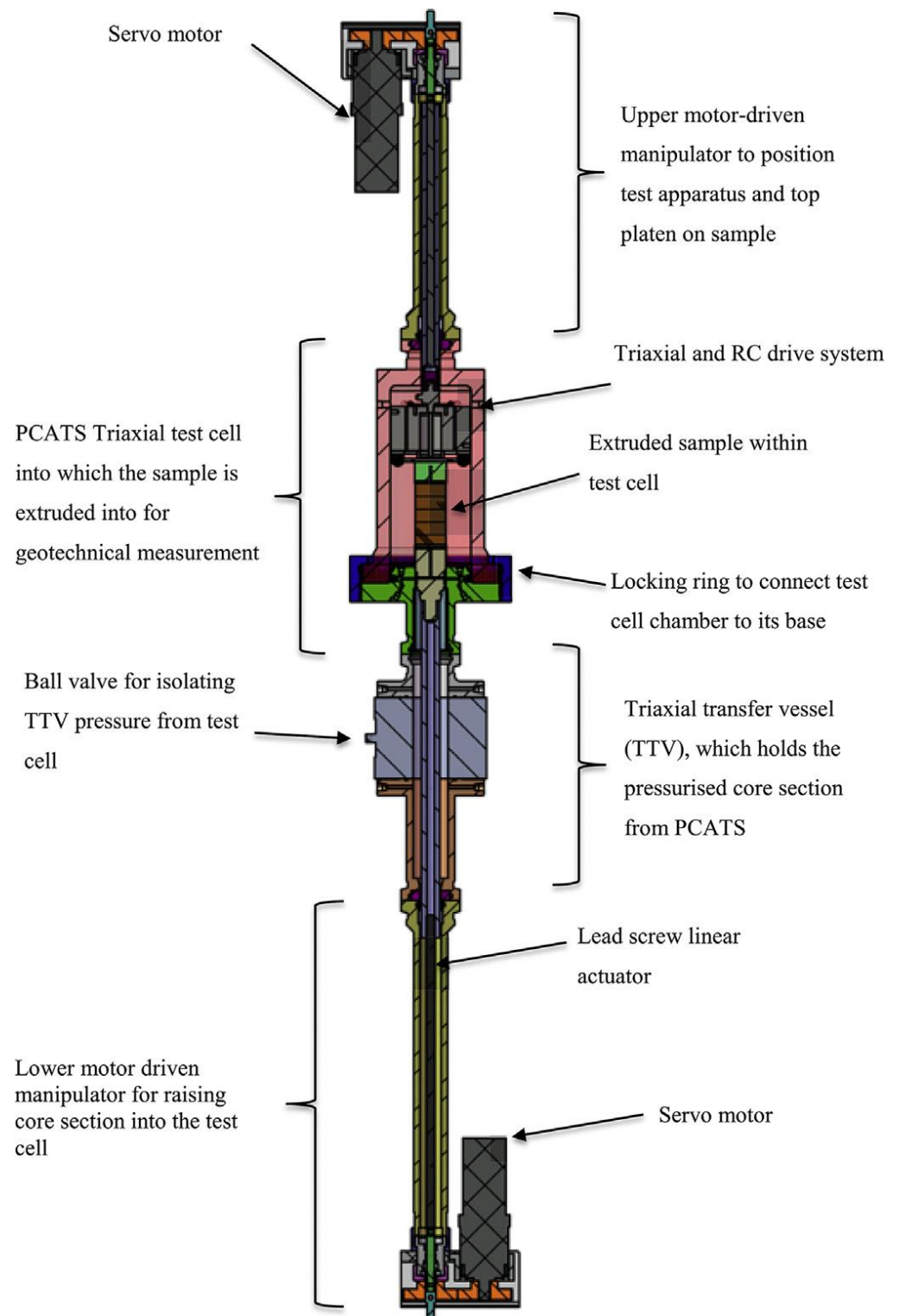
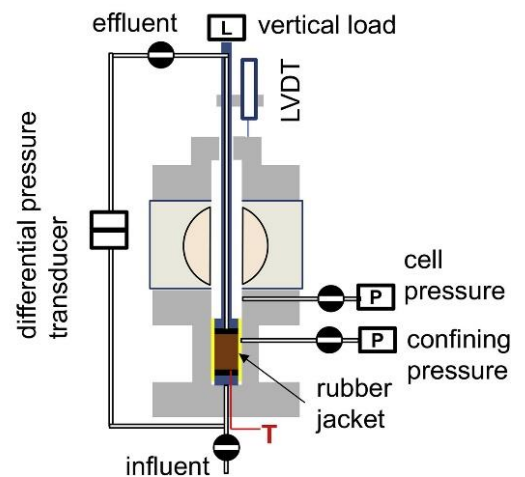
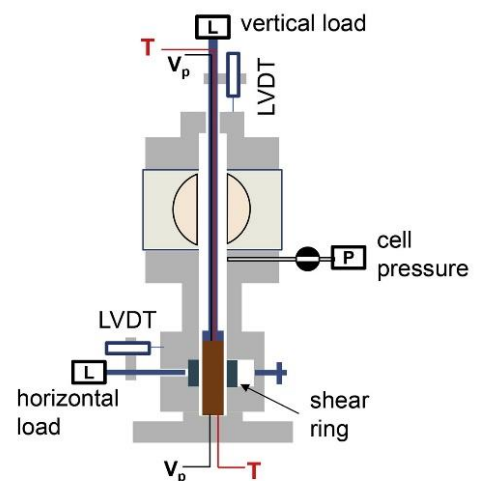
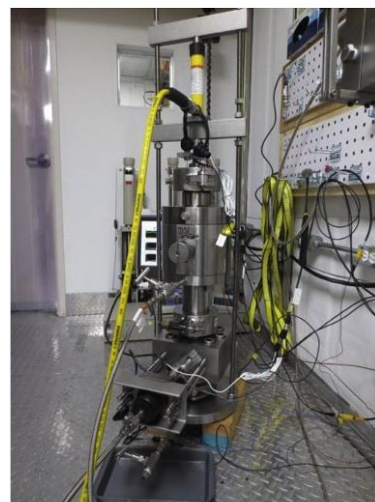


Figure 9. Diagram of pressure core analysis and transfer system (PCATS) triaxial (Reprinted with permission from Ref. [54], 2015, Elsevier).



(a) ESC



(b) DSC

Figure 10. Pressure-holding core characterization tool with effective stress chamber and direct shear chamber (Reprinted with permission from Ref. [103]. 2019, Elsevier): (a) the effective stress chamber, ESC; (b) the direct shear chamber, DSC.

2.3. Current Progress of Direct Shear in HBS

The horizontal deformation of HBS would influence the stability of the wellbore and the safety of a drilling platform [104,105]. Therefore, studying the horizontal shear mechanical properties of hydrate reservoirs is of great significance in avoiding the occurrence of geological disasters such as subsea wellbore collapse, instability, and submarine slides [106]. For understanding the horizontal deformation of HBS, the direct shear instrument has been widely used in horizontal shear mechanical testing [107,108].

Due to the special temperature and pressure conditions of hydrate synthesis, the conventional direct shear device was modified (that is, a thermal insulation system and a methane supply system were added) to test the horizontal mechanical behavior of HBS [109,110]. Liu et al. (2018) reported a direct shear instrument consisting of a shear box, a horizontal-displacement-test module, an axial-compression loading module, a temperature-control module, an air-supply module and a data-acquisition module; related information is shown in Table 3 and Figure 11. A series of direct shear tests of sandy and silty CO_2 hydrates showed that the hydrate-free sediments do not exhibit a peak during the entire

shearing process. However, the peak strength of sandy hydrates occurred when horizontal displacement was 1 mm, and that of silty hydrate sediments occurred when the horizontal displacement was 2–4 mm [30]. For the in-situ mechanical study of hydrates in the Nankai Trough of Japan, a direct shear chamber was equipped with the pressure core characterization system. In this device, the pressure core sample size was $\Phi 7.9 \times 50.8$ mm, and the maximum shear displacement was 15 mm, allowing both the peak and residual shear strengths to be determined [111]. The results showed that the strength and peak shear angle of never-depressurized pressure-core samples were larger than that of the post-dissociation samples, while the residual friction angle remained unchanged in both samples [110].

Table 3. Parameters of direct shear instrument.

Sample Size (mm)	Temperature Control Capability (°C)	Temperature Precision (°C)	Shear Transmission Mode	Vertical Loading	Reference
$\Phi 61.8 \times 20$	−20–150	± 0.5	Hydraulic transmission (16 t)	Piston Rod (Pneumatic Transmission)	Liu et al. (2017) [109]



Figure 11. Diagram of the direct shear system [30].

In summary, there are a few reports on the horizontal mechanical study in HBS and these are mainly on the shear mechanical properties of synthetic HBS. Due to the complexity and high cost of the pressure-core, the in-situ direct shear device was mainly incorporated with other mechanical instruments to obtain multiple mechanical parameters of a single sample.

2.4. Development of Ring Shear Test Method

For obtaining the residual strength of rocks in larger deformation, the ring-shear instrument has been widely used in analyses of the failure mechanism of landslides [112]. Ring-shear mechanical tests have been used to evaluate the rheology of powder [113], the residual strength, and the mechanical evolution mechanism of particles under long-distance migration [114]. The triaxial and direct shear tests have the advantages of depicting the elastoplastic deformation behavior of HBS. However, the residual strength of HBS in a larger deformation is difficult to obtain using them.

Submarine landslide is a potential risk to commercial production of hydrate. To test the residual strength of HBS under larger deformations, such as submarine landslides, some scholars [31,115] have performed some basic work on the development of ring-shear devices and mechanical research (Table 4). Spangenberg et al. (2020) developed a constant-temperature ring-shear instrument to determine the residual strength of hydrate or ice-containing sediments (Figure 12) [31]. The maximum hydraulic pressure resistance of this apparatus is 30 MPa.

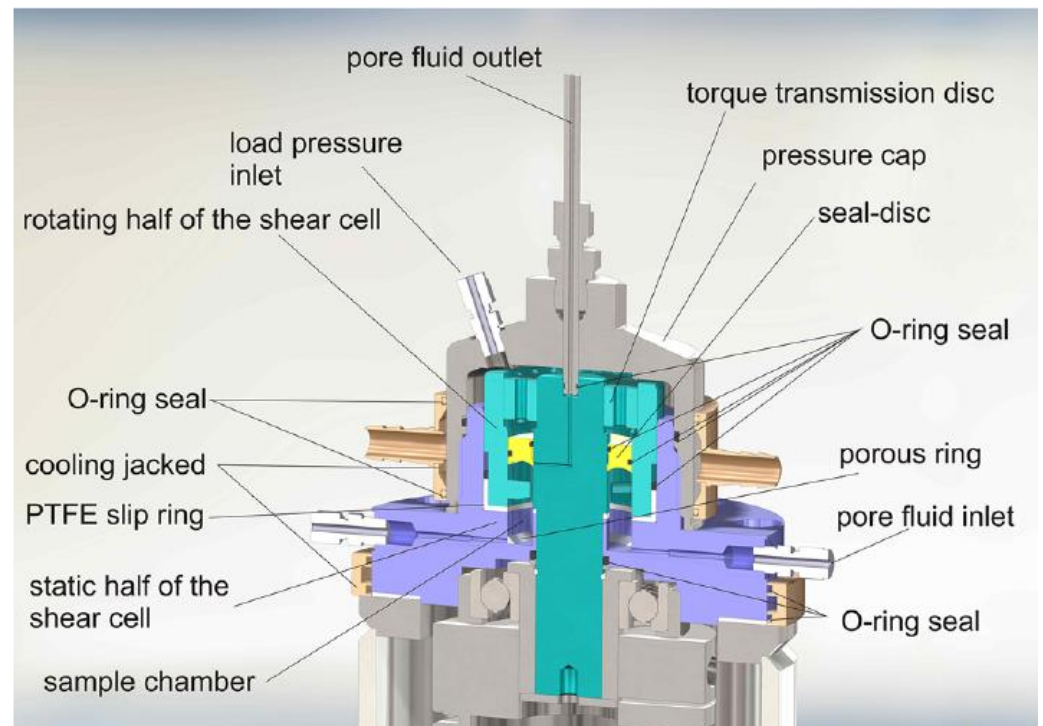


Figure 12. Schematic diagram of a section of ring-shear device (Reprinted with permission from Ref. [31]. 2020, American Institute of Physics).

Kimura et al. [116] developed a ring-shear test instrument that could test the permeability of different mineral hydrates under different normal stresses, in addition to the residual strength. The test results showed that, when the normal stress was 0.5–3 MPa, the permeability of the Toyoura sand hydrate decreased rapidly with increasing normal stress, and the permeability rate decreased with increasing normal stress when it exceeded 3 MPa. The permeability of silica sand hydrate decreased rapidly with the increase in normal stress when it was 0.5–2 MPa. To study the effect of effective normal stress on sand fragmentation, porosity, and permeability, the ring-shear instrument was used to investigate the mechanical behavior of HBS with the fault [117]. To further study the effect of the development of fault structures on the permeability of the Nankai Trough in Japan, Kimura et al. (2019) studied the evolution of the permeability of unconsolidated turbidite sand sediments during the shear process of the ring [115]. The results showed that the permeability clearly decreased when the shear displacement was 0.2–0.5 m, and then slowly decreased with increasing shear displacement until the shear displacement reached 10 m. The permeability decreased by 3–4 orders of magnitude after shear compared to before shear.

Table 4. Basic parameters of ring shear.

References	Inside Diameter (mm)	Outside Diameter (mm)	Height (mm)	Maximum Normal Loading (MPa)	Shear Ratios (mm/min)	Normal Loading Method
Kimura et al. (2014) [117]	55	75	20	10	0.2–1020	pneumatic piston
Spangenberg et al. (2020) [31]	30	50	25 ± 5	30	0.08–4.0	hydraulic piston

In summary, the ring shear is greatly important in obtaining the residual strength of HBS, but it still has many limitations, such as it cannot consider a load of ocean current disturbance, extreme earthquakes, and casing vibration during hydrate production. In the

future, the dynamic processes of hydrate decomposition, sand production, creep instability, and large-scale landslides in hydrate exploitation are recommended to be considered in the development of ring shear instruments. In addition, bender element and mechanical vibration are potential choices to be integrated with ring shear for researching the coupling mechanism of multiphysics.

2.5. Cone-Penetration Testing Method

The static-penetration-test technology (SPTC) is an in-situ test technology. To evaluate the mechanical properties of the soil at different depths during the pressing process, a penetration rod equipped with a sensor was developed [118]. SPTC has been applied in soft-soil-foundation bearing-capacity estimation, consolidation history inversion, and pile foundation evaluation [119–121].

Concerning the in-situ mechanical test of the hydrate reservoir, there have been a few reports of SPTC due to its complex operation process and high cost in the deep sea. Wang et al. (2019) discussed the development direction of SPTC in hydrate exploration and the feasibility of investigating hydrate distribution and reserves [122]. To determine the engineering mechanical properties of HBS, the Qingdao Institute of Marine Geology of China developed an SPTC system that integrated static penetration and cross-plate shear technology [123]. The tip resistance and shear strength of HBS at different depths can be obtained by using this system (Figure 13). Li et al. (2020) introduced the functions of this system and performed a series of functional verification experiments [124]. Its reliability was verified by the comparison of field-measured data of the silt clay layer in the Shenhu area of the South China Sea and experimental results.

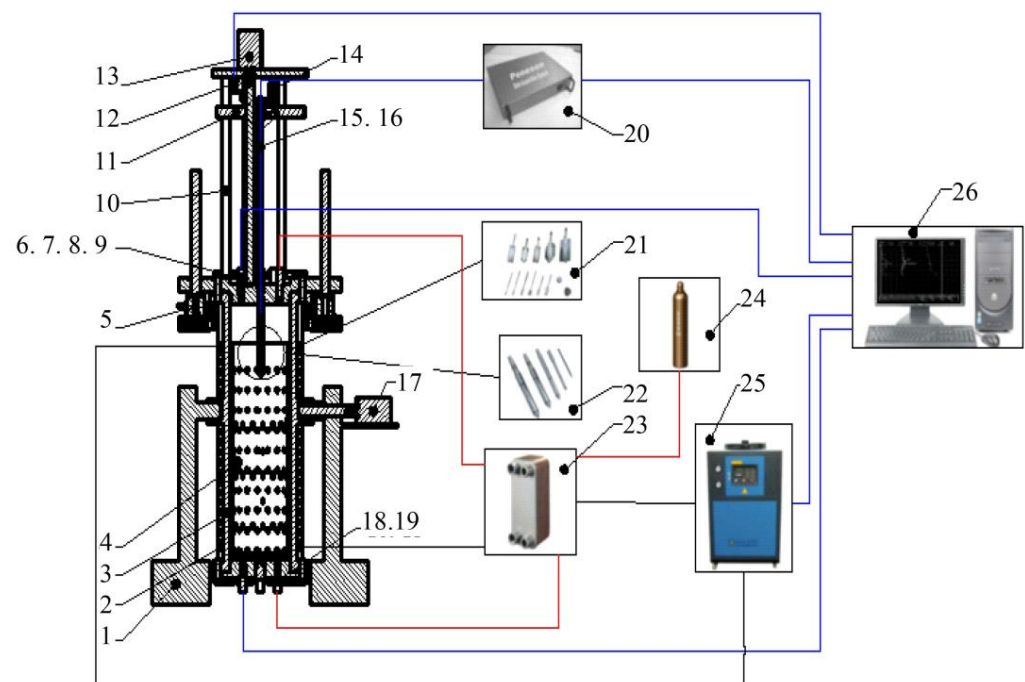


Figure 13. Diagram of engineering geological parameters of gas hydrate evaluation system [123,124]: 1. flip scaffold; 2. condenser pipe and insulation layer; 3. chamber; 4. inner bladder; 5. open lift; 6. sensors of cover; 7. valves of cover; 8. watertight insert; 9. rod dynamic seal and rotary seal; 10. guide rod and reaction force support frame; 11. briguette; 12. depth encoder; 13. penetration motor; 14. torsion motor; 15. probe; 16. probe cable; 17. rotating motor of chamber; 18. sensors under the cover; 19. valves under the cover; 20. data collector; 21. cross plate probe; 22. static penetration probe; 23. plate heat exchanger; 24. methane; 25. refrigerator; 26. computer.

In conclusion, to evaluate the mechanics of the hydrate reservoir, laboratory multiple function mechanical testing devices, which integrate static penetration with cross-plate test

technology, have been developed. However, the measurement data was less reported concerning this instrument. Additionally, for this static penetration platform, the relationship between test results and actual reservoir results needs to be further clarified.

In future instrument development, static penetration and cross plate can integrate with a deep-water robot to implement in-situ testing of static cone penetration or cross shear, supporting basic data for failure mechanical research of reservoirs.

3. Discussion

To predict the potential disaster risk (i.e., local instability, wellbore slumps, seabed subsidence, and large-scale submarine landslides) caused by hydrate production, many instruments have been developed to measure the mechanical properties of HBS. Although these test methods help advance the study of HBS mechanics, there are still many limitations and challenges in the mechanical tests of HBS.

3.1. On the Cross-Scale Analysis of Mechanical Properties of HBS

For testing the mechanical properties of HBS from small deformation to larger deformations, the HBS mechanical test instruments are mainly concentrated on the triaxial shear, supplemented by other instruments (i.e., bender element, ring shear, and direct shear, etc.), as shown in Figure 14. Among them, the sample height of CT scanning, ring shear, and direct shear is relatively small, while the sample size range of triaxial shear is wider, and the height of pressure core samples and resonance column samples is generally larger. Pressure-core testing technology and CT-scanning imaging technology are significant in sampling and imaging. The strain test range is ranked from small to large in bending element, resonance column, small strain triaxial, CT scanning, pressure core, triaxial shear, direct shear, and ring shear. Since CT scanning and pressure core are usually used in integrating with a triaxial shear instrument, the strain test range is equivalent to that of the triaxial shear.

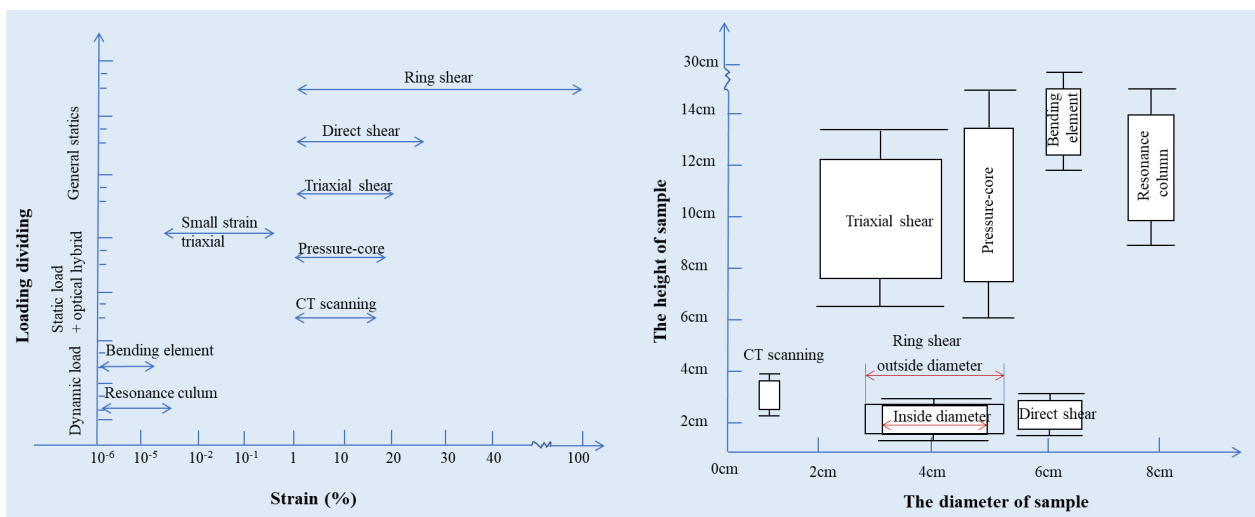


Figure 14. Test instrument performance comparison.

In summary, a mechanical research pattern from elastic deformation to plastic failure deformation of HBS has formed. However, there are still many limitations to these test methods:

- (1) Currently, mechanical tests focus mainly on the short-term failure of HBS, lacking comparability in the mechanical properties obtained from different experiments. Even for a widely used test method such as triaxial shear, there is no unified standard in sample synthesis and error analysis. In addition, no study considers the effect of sample size on the mechanics of HBS, and it remains to be clarified whether

the mechanical parameters measured by various experimental instruments can be directly used in the reservoir deformation simulation of hydrate production at trial. Therefore, strengthening the formulation of relevant test-process specifications and increasing the development of unified standard sample preparation equipment would be recommended. The innovation in the hydrate synthesis method for clayey-silt sediments needs to be strengthened, mainly to solve the difficulty of hydrate synthesis in in-situ seabed soil.

- (2) At present, most of the synthetic samples, assuming that all gas or liquid is consumed during synthesis, used for hydrate mechanical tests are homogeneous. Due to a lack of monitoring of hydrate distribution after sample synthesis, mechanical test values may deviate from true values. Therefore, improving the monitoring technology for hydrate distribution would be of great importance in quantifying the relationship between hydrate heterogeneity and mechanical properties. Furthermore, research on the heterogeneity of hydrate sediments is mainly based on numerical simulation, and the mechanical properties of heterogeneous samples are still unclear, as a result of the lack of experimental results.
- (3) In-situ mechanical results of hydrate reservoirs often only reflect the mechanical properties of sediments at specific sampling points at different depths, lacking sufficient data of different sites in the overall understanding of the mechanical behavior of the reservoirs. In addition, in-situ lateral mechanical test instruments and related mechanical theories urgently need to make breakthroughs considering the wellbore.

3.2. Main Challenges and Development Tendency

Although current mechanical test methods for HBS are constantly being enriched, they still cannot meet all the needs of the various complex working conditions of hydrate production. The challenges faced are as follows:

- (1) Defining and clarifying the feasibility of experimental test results to guide trial production is a major challenge for future hydrate mechanical research. The ratio between experimental results and monitoring results on site is unclear and there are many uncertainties about whether the experimental results can reflect the mechanical characteristics of an actual hydrate reservoir. Whether the laboratory test results can be directly used to predict the mechanical failure of field reservoirs remains unclear, and it is difficult to eliminate the public concerns about the development of hydrates that may lead to geological disasters and environmental problems.
- (2) How to unify the mechanical parameters obtained by various testing methods and form an overall understanding of the mechanical properties of HBS is another major challenge for the future mechanical test theories of HBS. Current mechanical tests just focus on the single deformation progress of HBS under a specific condition, while the mechanical progress from small-strain deformation to large-scale slides is a progressive process.
- (3) Monitoring the creep mechanics of field hydrate reservoirs and simulating the creep deformation under production conditions in the laboratory will be another challenge for future HBS mechanical test methods. In the process of hydrate production, the creep mechanical progress of HBS is a multi-physics coupling process, and clarifying its evolution mechanism is the key to judging whether a reservoir will undergo creep failure. However, the mechanical means of a hydrate sediment creep test is mainly the triaxial shear and other test equipment and theory is lacking.

4. Conclusions and Suggestions

This study summarized the progress of laboratory testing methods and mechanical research for the mechanical properties of HBS. The basic performance of each mechanical test technique was compared, from small-strain deformation to residual-deformation testing.

For acquiring the mechanical properties of HBS under different stress conditions, a basic pattern is formed mainly around triaxial shear and supplemented by direct shear,

resonance column, and ring shear. As the in-situ mechanical test still has limitations in the high cost and difficulty of technology, the more economical test methods are mainly indoor experiment simulation. Therefore, the technical upgrading and theoretical innovation of hydrate sediments could be carried out from the following aspects:

- (1) It is necessary to formulate and improve the relevant operating specifications of the existing test methods, clarifying the correlation between the test results and the real mechanical properties of the reservoir. Heterogeneity is an inherent property of hydrate reservoirs; the research on the mechanical properties of heterogeneous hydrate sediments should be strengthened.
- (2) In the future, the development trend of hydrate mechanical test instruments should develop toward high precision, multifunctional integration, which requires strong theoretical coupling between each test module. Therefore, both experimental and numerical simulation analyses of hydrate reservoirs require a unified theory in depicting different mechanical deformation processes.
- (3) There is an urgent need for comprehensive cross-scale analyses of the mechanical properties of HBS, solving the theoretical problems faced in the usability between experimental results obtained by varying mechanical instruments and field trials.

Author Contributions: Idea, Y.L. and N.W.; methodology, Y.L., N.W. and M.C.; data analysis, Q.H., Y.Z. and G.Y.; investigation, M.C., Y.L. and H.J.; writing—original draft preparation, M.C. and Y.L.; writing—review and editing, Y.L., L.D., Ş.M. and Y.Z. All authors have read and agreed to the published version of the manuscript.

Funding: The authors wish to gratefully acknowledge the financial support of the National Natural Science Foundation of China (grant number: 41976074, 42076217), and the Taishan Scholar Special Experts Project of Shandong Province (grant number: ts201712079).

Conflicts of Interest: The authors declare that we have no known conflict interests or personal relationships that could have appeared to influence the work reported in this paper.

References

1. Feng, Y.; Chen, L.; Suzuki, A.; Kogawa, T.; Okajima, J.; Komiya, A.; Maruyama, S. Numerical analysis of gas production from layered methane hydrate reservoirs by depressurization. *Energy* **2019**, *166*, 1106–1119. [[CrossRef](#)]
2. Yu, T.; Guan, G.; Abudula, A. Production performance and numerical investigation of the 2017 offshore methane hydrate production test in the Nankai Trough of Japan. *Appl. Energy* **2019**, *251*, 113338. [[CrossRef](#)]
3. Yu, T.; Guan, G.; Abudula, A.; Yoshida, A.; Wang, D.; Song, Y. Application of horizontal wells to the oceanic methane hydrate production in the Nankai Trough, Japan. *J. Nat. Gas Sci. Eng.* **2019**, *62*, 113–131. [[CrossRef](#)]
4. Boswell, R. Is Gas Hydrate Energy Within Reach? *Science* **2009**, *325*, 957–958. [[CrossRef](#)] [[PubMed](#)]
5. Wang, L.; Zhao, J.; Sun, X.; Wu, P.; Shen, S.; Liu, T.; Li, Y. Comprehensive review of geomechanical constitutive models of gas hydrate-bearing sediments. *J. Nat. Gas Sci. Eng.* **2021**, *88*, 103755. [[CrossRef](#)]
6. Wu, P.; Li, Y.; Sun, X.; Liu, W.; Song, Y. Mechanical Characteristics of Hydrate-Bearing Sediment: A Review. *Energy Fuels* **2021**, *35*, 1041–1057. [[CrossRef](#)]
7. Merey, S.; Sinayuc, C. Investigation of gas hydrate potential of the Black Sea and modelling of gas production from a hypothetical Class 1 methane hydrate reservoir in the Black Sea conditions. *J. Nat. Gas Sci. Eng.* **2016**, *29*, 66–79. [[CrossRef](#)]
8. Li, Y.; Liu, C.; Liu, L.; Sun, J.; Liu, H.; Meng, Q. Experimental study on evolution behaviors of triaxial-shearing parameters for hydrate-bearing intermediate fine sediment. *Adv. Geo-Energy Res.* **2018**, *2*, 43–52. [[CrossRef](#)]
9. Li, Y.; Hu, G.; Wu, N.; Liu, C.; Chen, Q.; Li, C. Undrained shear strength evaluation for hydrate-bearing sediment overlying strata in the Shenhu area, northern South China Sea. *Acta Oceanol. Sin.* **2019**, *38*, 114–123. [[CrossRef](#)]
10. Zhang, M.; Niu, M.; Shen, S.; Dai, S.; Xu, Y. Review of natural gas hydrate dissociation effects on seabed stability. *Nat. Hazards* **2021**, *107*, 1035–1045. [[CrossRef](#)]
11. He, Y.; Zhong, G.; Wang, L.; Kuang, Z. Characteristics and occurrence of submarine canyon-associated landslides in the middle of the northern continental slope, South China Sea. *Mar. Pet. Geol.* **2014**, *57*, 546–560. [[CrossRef](#)]
12. Zhou, W.; Wang, Y.; Gao, X.; Zhu, W.; Xu, Q.; Xu, S.; Cao, J.; Wu, J. Architecture, evolution history and controlling factors of the Baiyun submarine canyon system from the middle Miocene to Quaternary in the Pearl River Mouth Basin, northern South China Sea. *Mar. Pet. Geol.* **2015**, *67*, 389–407. [[CrossRef](#)]
13. Chen, D.; Wang, X.; Völker, D.; Wu, S.; Wang, L.; Li, W.; Li, Q.; Zhu, Z.; Li, C.; Qin, Z.; et al. Three dimensional seismic studies of deep-water hazard-related features on the northern slope of South China Sea. *Mar. Pet. Geol.* **2016**, *77*, 1125–1139. [[CrossRef](#)]

14. Sun, Q.; Cartwright, J.; Wu, S.; Zhong, G.; Wang, S.; Zhang, H. Submarine erosional troughs in the northern South China Sea: Evidence for Early Miocene deepwater circulation and paleoceanographic change. *Mar. Pet. Geol.* **2016**, *77*, 75–91. [[CrossRef](#)]
15. Li, Y.; Wu, N.; Ning, F.; Gao, D.; Hao, X.; Chen, Q.; Liu, C.; Sun, J. Hydrate-induced clogging of sand-control screen and its implication on hydrate production operation. *Energy* **2020**, *206*, 118030. [[CrossRef](#)]
16. Freij-Ayoub, R.; Tan, C.; Clennell, B.; Tohidi, B.; Yang, J. A wellbore stability model for hydrate bearing sediments. *J. Pet. Sci. Eng.* **2007**, *57*, 209–220. [[CrossRef](#)]
17. Kim, A.R.; Kim, J.T.; Cho, G.C.; Lee, J.Y. Methane Production from Marine Gas Hydrate Deposits in Korea: Thermal-Hydraulic-Mechanical Simulation on Production Wellbore Stability. *J. Geophys. Res. Solid Earth* **2018**, *123*, 9555–9569. [[CrossRef](#)]
18. Yang, L.; Wang, J.; Yang, Y.; Sun, G. Numerical Analysis of Soil Deformation and Collapse Due to Hydrate Decomposition. *ACS Omega* **2021**, *6*, 5335–5347. [[CrossRef](#)]
19. Aydin, H.; Merey, S. The effect of gas production from deeper conventional gas reservoirs on shallower gas hydrate layer stability: A case study in the conditions of the Sakarya gas field, Western Black Sea. *J. Nat. Gas Sci. Eng.* **2021**, *94*, 104103. [[CrossRef](#)]
20. Dong, L.; Li, Y.; Liao, H.; Liu, C.; Chen, Q.; Hu, G.; Liu, L.-L.; Meng, Q. Strength estimation for hydrate-bearing sediments based on triaxial shearing tests. *J. Pet. Sci. Eng.* **2020**, *184*, 106478. [[CrossRef](#)]
21. Dong, L.; Li, Y.; Liu, C.; Liao, H.; Chen, G.; Chen, Q.; Liu, L.; Hu, G. Mechanical Properties of Methane Hydrate-Bearing Interlayered Sediments. *J. Ocean Univ. China* **2019**, *18*, 1344–1350. [[CrossRef](#)]
22. Li, Y.-H.; Song, Y.-C.; Yu, F.; Liu, W.-G.; Zhao, J.-F. Experimental study on mechanical properties of gas hydrate-bearing sediments using kaolin clay. *China Ocean Eng.* **2011**, *25*, 113–122. [[CrossRef](#)]
23. Miyazaki, K.; Masui, A.; Sakamoto, Y.; Aoki, K.; Temma, N.; Yamaguchi, T. Triaxial compressive properties of artificial methane-hydrate-bearing sediment. *J. Geophys. Res. Solid Earth* **2011**, *116*, B06102. [[CrossRef](#)]
24. Hyodo, M.; Li, Y.; Yoneda, J.; Nakata, Y.; Yoshimoto, N.; Nishimura, A.; Song, Y. Mechanical behavior of gas-saturated methane hydrate-bearing sediments. *J. Geophys. Res. Solid Earth* **2013**, *118*, 5185–5194. [[CrossRef](#)]
25. Dong, L.; Wan, Y.; Li, Y.; Liao, H.; Liu, C.; Wu, N.; Leonenko, Y. 3D numerical simulation on drilling fluid invasion into natural gas hydrate reservoirs. *Energy* **2022**, *241*, 122932. [[CrossRef](#)]
26. Zhao, Y.; Liu, L.; Kong, L.; Liu, C.; Wu, N. Advances in Micromechanical Properties of Hydrate-Bearing Soils. *Chin. J. Theor. Appl. Mech.* **2021**, *53*, 2119–2140.
27. Lee, J.Y.; Francisca, F.M.; Santamarina, J.C.; Ruppel, C. Parametric study of the physical properties of hydrate-bearing sand, silt, and clay sediments: 2. Small-strain mechanical properties. *J. Geophys. Res. Solid Earth* **2010**, *115*, B11105. [[CrossRef](#)]
28. Liu, Z.; Kim, J.; Hu, G.; Hu, W.; Ning, F. Geomechanical property evolution of hydrate-bearing sediments under dynamic loads: Nonlinear behaviors of modulus and damping ratio. *Eng. Geol.* **2021**, *295*, 106427. [[CrossRef](#)]
29. Li, Y.; Dong, L.; Wu, N.; Nouri, A.; Liao, H.; Chen, Q.; Sun, J.; Liu, C. Influences of hydrate layered distribution patterns on triaxial shearing characteristics of hydrate-bearing sediments. *Eng. Geol.* **2021**, *294*, 106375. [[CrossRef](#)]
30. Liu, Z.; Dai, S.; Ning, F.; Peng, L.; Wei, H.; Wei, C. Strength Estimation for Hydrate-Bearing Sediments from Direct Shear Tests of Hydrate-Bearing Sand and Silt. *Geophys. Res. Lett.* **2018**, *45*, 715–723. [[CrossRef](#)]
31. Spangenberg, E.; Heeschen, K.U.; Giese, R.; Schicks, J.M. “Ester”—A new ring-shear-apparatus for hydrate-bearing sediments. *Rev. Sci. Instrum.* **2020**, *91*, 064503. [[CrossRef](#)] [[PubMed](#)]
32. Sultan, N.; Garziglia, S. Geomechanical constitutive modelling of gas-hydrate-bearing sediments. In Proceedings of the 7th International Conference on Gas Hydrates, Edinburgh, UK, 17–21 July 2011.
33. Nakashima, K.; Nakata, Y.; Hyodo, M.; Yoshimoto, N.; Hiraoka, S.; Kajiyama, S. Compressive characteristics of methane hydrate-bearing sands under isotropic consolidation. *Soils Found.* **2021**, *61*, 506–519. [[CrossRef](#)]
34. Ye, Y. *Development of the Experiment Detection Technique*; Springer: Berlin/Heidelberg, Germany, 2012; pp. 19–87.
35. Ye, Y.; Liu, C. *Natural Gas Hydrates: Experimental Techniques and Their Applications*; Springer-Verlag: Berlin/Heidelberg, Germany, 2013.
36. Khan, Q.; Subramanian, S.; Wong, D.Y.; Ku, T. Bender elements in stiff cemented clay: Shear wave velocity (V_s) correction by applying wavelength considerations. *Can. Geotech. J.* **2019**, *56*, 1034–1041. [[CrossRef](#)]
37. Lee, J.-S.; Santamarina, J.C. Bender Elements: Performance and Signal Interpretation. *J. Geotech. Geoenviron. Eng.* **2005**, *131*, 1063–1070. [[CrossRef](#)]
38. Hu, G.-W.; Ye, Y.-G.; Zhang, J.; Diao, S.-B.; Liu, C.-L. Acoustic Properties of Hydrate-Bearing Unconsolidated Sediments Measured by the Bender Element Technique. *Chin. J. Geophys.* **2012**, *55*, 635–647. [[CrossRef](#)]
39. Meixiu, J.; Yunin, C.; Bo, H. Method for precisely determining shear wave velocity of soil from bender element tests. *Chin. J. Geotech. Eng.* **2003**, *25*, 732–736.
40. Hu, G.; Ye, Y.; Zhang, J.; Liu, C.; Li, Q. Acoustic response of gas hydrate formation in sediments from South China Sea. *Mar. Pet. Geol.* **2014**, *52*, 1–8. [[CrossRef](#)]
41. Ji, L.; Chiu, A.C.; Ma, L.; Jian, C. *Shear Modulus of Hydrate Bearing Calcareous Sand-Fines Mixture*; EDP Sciences: Les Ulis, France, 2019.
42. Kim, H.-S.; Cho, G.-C.; Kwon, T.-H. Effect of CO₂ hydrate formation on seismic wave velocities of fine-grained sediments. *Geochem. Geophys. Geosyst.* **2013**, *14*, 1787–1799. [[CrossRef](#)]
43. Guler, E.; Afacan, K.B. Dynamic behavior of clayey sand over a wide range using dynamic triaxial and resonant column tests. *Geomech. Eng.* **2021**, *24*, 105–113.

44. Nakagawa, S. Split Hopkinson resonant bar test for sonic-frequency acoustic velocity and attenuation measurements of small, isotropic geological samples. *Rev. Sci. Instrum.* **2011**, *82*, 044901. [[CrossRef](#)]
45. Song, B.; Tsinaris, A.; Anastasiadis, A.; Ptilakis, K.; Chen, W. Small-strain stiffness and damping of Lanzhou loess. *Soil Dyn. Earthq. Eng.* **2017**, *95*, 96–105. [[CrossRef](#)]
46. Patiño, H.; Martínez, E.; Galindo, R. Dynamic Behavior of a Granular Medium Subjected to Resonant Column Tests: Application to Ottawa Sand. *Geotech. Test. J.* **2020**, *43*, 132–150. [[CrossRef](#)]
47. Cascante, G.; Santamarina, C.; Yassir, N. Flexural excitation in a standard torsional-resonant column device. *Can. Geotech. J.* **1998**, *35*, 478–490. [[CrossRef](#)]
48. Schaeffer, K.; Bearce, R.; Wang, J. Dynamic Modulus and Damping Ratio Measurements from Free-Free Resonance and Fixed-Free Resonant Column Procedures. *J. Geotech. Geoenviron. Eng.* **2013**, *139*, 2145–2155. [[CrossRef](#)]
49. Wang, X.; Xia, T.; Zhang, L.; Ding, Z.; He, S.; Peng, Y. Effect of soil microstructure on the small-strain shear modulus of saline soil. *Arab. J. Geosci.* **2021**, *14*, 1. [[CrossRef](#)]
50. Liu, Z.; Ning, F.; Hu, G.; Liu, L.; Liu, C.; Peng, L.; Wang, D.; Hu, W.; Zhang, Z. Characterization of seismic wave velocity and attenuation and interpretation of tetrahydrofuran hydrate-bearing sand using resonant column testing. *Mar. Pet. Geol.* **2020**, *122*, 104620. [[CrossRef](#)]
51. Priest, J.A.; Rees, E.V.L.; Clayton, C.R.I. Influence of gas hydrate morphology on the seismic velocities of sands. *J. Geophys. Res. Solid Earth* **2009**, *114*, B11205. [[CrossRef](#)]
52. Sultaniya, A.K.; Priest, J.A.; Clayton, C.R.I. Measurements of the changing wave velocities of sand during the formation and dissociation of disseminated methane hydrate. *J. Geophys. Res. Solid Earth* **2015**, *120*, 778–789. [[CrossRef](#)]
53. Priest, J.A.; Best, A.I.; Clayton, C.R.I. Attenuation of seismic waves in methane gas hydrate-bearing sand. *Geophys. J. Int.* **2006**, *164*, 149–159. [[CrossRef](#)]
54. Priest, J.A.; Druce, M.; Roberts, J.; Schultheiss, P.; Nakatsuka, Y.; Suzuki, K. PCATS Triaxial: A new geotechnical apparatus for characterizing pressure cores from the Nankai Trough, Japan. *Mar. Pet. Geol.* **2015**, *66*, 460–470. [[CrossRef](#)]
55. Liu, Z.; Kim, J.; Lei, L.; Ning, F.; Dai, S. Tetrahydrofuran Hydrate in Clayey Sediments—Laboratory Formation, Morphology, and Wave Characterization. *J. Geophys. Res. Solid Earth* **2019**, *124*, 3307–3319. [[CrossRef](#)]
56. Wang, D.; Liu, Z.; Ning, F.; Hu, W.; Peng, L.; Hu, G.; Zhang, Z.; Luo, Q.; Li, X.; Dou, X.; et al. Dynamic responses of THF hydrate-bearing sediments under small strain: Resonance column test. *J. Nat. Gas Sci. Eng.* **2020**, *81*, 103399. [[CrossRef](#)]
57. Clayton, C.R.I.; Priest, J.A.; Best, A.I. The effects of disseminated methane hydrate on the dynamic stiffness and damping of a sand. *Geotechnique* **2005**, *55*, 423–434. [[CrossRef](#)]
58. Priest, J.; Best, A.I.; Clayton, C.R.I. A laboratory investigation into the seismic velocities of methane gas hydrate-bearing sand. *J. Geophys. Res. Solid Earth* **2005**, *110*, B04102. [[CrossRef](#)]
59. Best, A.I.; Priest, J.; Clayton, C.R.I.; Rees, E.V.L. The effect of methane hydrate morphology and water saturation on seismic wave attenuation in sand under shallow sub-seafloor conditions. *Earth Planet. Sci. Lett.* **2013**, *368*, 78–87. [[CrossRef](#)]
60. Yamamoto, K. Overview and introduction: Pressure core-sampling and analyses in the 2012–2013 MH21 offshore test of gas production from methane hydrates in the eastern Nankai Trough. *Mar. Pet. Geol.* **2015**, *66*, 296–309. [[CrossRef](#)]
61. Konno, Y.; Fujii, T.; Sato, A.; Akamine, K.; Naiki, M.; Masuda, Y.; Yamamoto, K.; Nagao, J. Key Findings of the World’s First Offshore Methane Hydrate Production Test off the Coast of Japan: Toward Future Commercial Production. *Energy Fuels* **2017**, *31*, 2607–2616. [[CrossRef](#)]
62. Yu, Y.; Luo, Q.; Ning, F.; Lu, H.; Liu, Z.; Peng, L.; Wang, D.; Shi, H.; Liu, Z.; Duan, L. Direct measurement of the interaction forces between sediment particles in gas hydrate reservoirs (in Chinese). *J. China Univ. Pet. (Ed. Nat. Sci.)* **2021**, *45*, 7.
63. Deng, Y.; Xu, L.; Lu, H.; Wang, H.; Shi, Y. Direct measurement of the contact angle of water droplet on quartz in a reservoir rock with atomic force microscopy. *Chem. Eng. Sci.* **2018**, *177*, 445–454. [[CrossRef](#)]
64. Peng, L.; Ning, F.; Li, W.; Cao, P.; Liu, Z.; Wang, D.; Zhang, Z.; Sun, J.; Zhang, L.; Jiang, G. Investigation on the effect of growth temperature and contact interface on surface characteristics of THF clathrate hydrates by atomic force microscopy (in Chinese). *Sci. Sin. Phys. Mech. Astron.* **2019**, *49*, 034612. [[CrossRef](#)]
65. Wood, E.L.; Avant, T.; Kim, G.S.; Lee, S.K.; Burchman, Z.; Hughes, J.M.; Sansoz, F. Size effects in bimetallic nickel–gold nanowires: Insight from atomic force microscopy nanoindentation. *Acta Mater.* **2014**, *66*, 32–43. [[CrossRef](#)]
66. Meiningner, G.A. The central importance of the cytoskeleton for increased cell stiffness in cardiovascular disease. Focus on “Diabetes increases stiffness of live cardiomyocytes measured by atomic force microscopy nanoindentation”. *Am. J. Physiol. Cell Physiol.* **2014**, *307*, C908. [[CrossRef](#)] [[PubMed](#)]
67. Guan, D.; Li, H.; Tong, P. Experimental methods and recent progress in biomechanics using atomic force microscopy. *J. Exp. Fluid Mech.* **2020**, *34*, 57–66.
68. Luo, T.; Li, Y.; Sun, X.; Shen, S.; Wu, P. Effect of sediment particle size on the mechanical properties of CH₄ hydrate-bearing sediments. *J. Pet. Sci. Eng.* **2018**, *171*, 302–314. [[CrossRef](#)]
69. Yun, T.S.; Santamarina, J.C.; Ruppel, C. Mechanical properties of sand, silt, and clay containing tetrahydrofuran hydrate. *J. Geophys. Res. Solid Earth* **2007**, *112*, B04106. [[CrossRef](#)]
70. Li, Y.; Liu, C.; Liao, H.; Lin, D.; Bu, Q.; Liu, Z. Mechanical properties of the clayey-silty sediment-natural gas hydrate mixed system. *Nat. Gas Ind. B* **2021**, *8*, 154–162. [[CrossRef](#)]

71. Li, Y.; Wu, N.; Gao, D.; Chen, Q.; Liu, C.; Yang, D.; Jin, Y.; Ning, F.; Tan, M.; Hu, G. Optimization and analysis of gravel packing parameters in horizontal wells for natural gas hydrate production. *Energy* **2021**, *219*, 119585. [[CrossRef](#)]
72. Luo, T.; Song, Y.; Zhu, Y.; Liu, W.; Liu, Y.; Li, Y.; Wu, Z. Triaxial experiments on the mechanical properties of hydrate-bearing marine sediments of South China Sea. *Mar. Pet. Geol.* **2016**, *77*, 507–514. [[CrossRef](#)]
73. Li, Y.; Liu, L.; Jin, Y.; Wu, N. Characterization and development of marine natural gas hydrate reservoirs in clayey-silt sediments: A review and discussion. *Adv. Geo-Energy Res.* **2021**, *5*, 75–86. [[CrossRef](#)]
74. Li, K.; Liu, R.-M.; Kong, L.; Zhao, X.-B. Modeling the Mechanical Behavior of Gas Hydrate Bearing Sediments Based on Unified Hardening Framework. *Geotech. Geol. Eng.* **2019**, *37*, 2893–2902. [[CrossRef](#)]
75. Song, Y.; Luo, T.; Madhusudhan, B.N.; Sun, X.; Liu, Y.; Kong, X.; Li, Y. Strength behaviors of CH₄ hydrate-bearing silty sediments during thermal decomposition. *J. Nat. Gas Sci. Eng.* **2019**, *72*, 103031. [[CrossRef](#)]
76. Yoneda, J.; Kida, M.; Konno, Y.; Jin, Y.; Morita, S.; Tenma, N. In Situ Mechanical Properties of Shallow Gas Hydrate Deposits in the Deep Seabed. *Geophys. Res. Lett.* **2019**, *46*, 14459–14468. [[CrossRef](#)]
77. Liu, J.-W.; Li, X.-S.; Kou, X.; Wang, Y.; Li, L.-J. Analysis of Hydrate Heterogeneous Distribution Effects on Mechanical Characteristics of Hydrate-Bearing Sediments. *Energy Fuels* **2021**, *35*, 4914–4924. [[CrossRef](#)]
78. Masui, A.; Haneda, H.; Ogata, Y.; Aoki, K. Effects of Methane Hydrate Formation On Shear Strength of Synthetic Methane Hydrate Sediments. In Proceedings of the Fifteenth International Offshore and Polar Engineering Conference, Seoul, Korea, 19–24 June 2005.
79. Xu, W.; Germanovich, L.N. Excess pore pressure resulting from methane hydrate dissociation in marine sediments: A theoretical approach. *J. Geophys. Res. Solid Earth* **2006**, *111*, B01104. [[CrossRef](#)]
80. Seol, Y.; Choi, J.-H.; Dai, S. Multi-property characterization chamber for geophysical-hydrological investigations of hydrate bearing sediments. *Rev. Sci. Instrum.* **2014**, *85*, 084501. [[CrossRef](#)]
81. Choi, J.H.; Dai, S.; Lin, J.S.; Seol, Y. Multistage Triaxial Tests on Laboratory-Formed Methane Hydrate-Bearing Sediments. *J. Geophys. Res. Solid Earth* **2018**, *123*, 3347–3357. [[CrossRef](#)]
82. Hyodo, M.; Li, Y.; Yoneda, J.; Nakata, Y.; Yoshimoto, N.; Nishimura, A. Effects of dissociation on the shear strength and deformation behavior of methane hydrate-bearing sediments. *Mar. Pet. Geol.* **2014**, *51*, 52–62. [[CrossRef](#)]
83. Yang, J.; Hassanpouryouzband, A.; Tohidi, B.; Chuvilin, E.; Bukhanov, B.; Istomin, V.; Cheremisin, A. Gas Hydrates in Permafrost: Distinctive Effect of Gas Hydrates and Ice on the Geomechanical Properties of Simulated Hydrate-Bearing Permafrost Sediments. *J. Geophys. Res. Solid Earth* **2019**, *124*, 2551–2563. [[CrossRef](#)]
84. Zhang, X.-H.; Wang, S.-Y.; Li, Q.-P.; Zhao, J.; Wang, A.-L. Experimental study of mechanical properties of gas hydrate deposits (in Chinese). *Chin. J. Rock Soil Mech.* **2010**, *31*, 3069–3074.
85. Guan, J.A.; Lu, J.; Lian, D.; Li, D.; Wan, L. Preliminary Tri-Axial Mechanical Test on the Hydrate-Bearing Media from Shenhu Area of South China Sea under High Confining Pressures. *Adv. New Renew. Energy* **2017**, *5*, 40–46.
86. Jin, Y.; Konno, Y.; Nagao, J. Pressurized subsampling system for pressured gas-hydrate-bearing sediment: Microscale imaging using X-ray computed tomography. *Rev. Sci. Instrum.* **2014**, *85*, 094502. [[CrossRef](#)]
87. Jin, Y.; Konno, Y.; Yoneda, J.; Kida, M.; Nagao, J. In Situ Methane Hydrate Morphology Investigation: Natural Gas Hydrate-Bearing Sediment Recovered from the Eastern Nankai Trough Area. *Energy Fuels* **2016**, *30*, 5547–5554. [[CrossRef](#)]
88. Yoneda, J.; Jin, Y.; Katagiri, J.; Tenma, N. Strengthening mechanism of cemented hydrate-bearing sand at microscales. *Geophys. Res. Lett.* **2016**, *43*, 7442–7450. [[CrossRef](#)]
89. Jin, S.; Takeya, S.; Hayashi, J.; Nagao, J.; Kamata, Y.; Ebinuma, T.; Narita, H. Structure Analyses of Artificial Methane Hydrate Sediments by Microfocus X-ray Computed Tomography. *Jpn. J. Appl. Phys.* **2004**, *43*, 5673–5675. [[CrossRef](#)]
90. Chen, X.; Verma, R.; Espinoza, D.N.; Prodanović, M. Pore-Scale Determination of Gas Relative Permeability in Hydrate-Bearing Sediments Using X-Ray Computed Micro-Tomography and Lattice Boltzmann Method. *Water Resour. Res.* **2018**, *54*, 600–608. [[CrossRef](#)]
91. Lei, L.; Gai, X.; Seol, Y. Load-bearing characteristic of methane hydrate within coarse-grained sediments—Insights from isotropic consolidation. *Mar. Pet. Geol.* **2020**, *121*, 104571. [[CrossRef](#)]
92. Lei, L.; Seol, Y. Pore-Scale Investigation of Methane Hydrate-Bearing Sediments Under Triaxial Condition. *Geophys. Res. Lett.* **2020**, *47*, e2019GL086448. [[CrossRef](#)]
93. Wu, P.; Li, Y.; Liu, W.; Liu, Y.; Wang, D.; Song, Y. Microstructure Evolution of Hydrate-Bearing Sands During Thermal Dissociation and Ensued Impacts on the Mechanical and Seepage Characteristics. *J. Geophys. Res. Solid Earth* **2020**, *125*, e2019JB019103. [[CrossRef](#)]
94. Wu, P.; Li, Y.; Liu, W.; Sun, X.; Kong, X.; Song, Y. Cementation Failure Behavior of Consolidated Gas Hydrate-Bearing Sand. *J. Geophys. Res. Solid Earth* **2020**, *125*, e2019JB018623. [[CrossRef](#)]
95. Ta, X.H.; Yun, T.S.; Muhunthan, B.; Kwon, T. Observations of pore-scale growth patterns of carbon dioxide hydrate using X-ray computed microtomography. *Geochem. Geophys. Geosyst.* **2015**, *16*, 912–924. [[CrossRef](#)]
96. Kerkar, P.B.; Horvat, K.; Jones, K.W.; Mahajan, D. Imaging methane hydrates growth dynamics in porous media using synchrotron X-ray computed microtomography. *Geochem. Geophys. Geosyst.* **2014**, *15*, 4759–4768. [[CrossRef](#)]
97. Chen, X.; Espinoza, D.N. Ostwald ripening changes the pore habit and spatial variability of clathrate hydrate. *Fuel* **2018**, *214*, 614–622. [[CrossRef](#)]

98. Mahabadi, N.; Dai, S.; Seol, Y.; Jang, J. Impact of hydrate saturation on water permeability in hydrate-bearing sediments. *J. Pet. Sci. Eng.* **2019**, *174*, 696–703. [[CrossRef](#)]
99. Wei, J.; Wu, T.; Feng, X.; Liang, J.; Li, W.; Xie, R.; Wu, G. Physical Properties of Gas Hydrate-Bearing Pressure Core Sediments in the South China Sea. *Geofluids* **2021**, *2021*, 1–10. [[CrossRef](#)]
100. Yoneda, J.; Masui, A.; Konno, Y.; Jin, Y.; Egawa, K.; Kida, M.; Ito, T.; Nagao, J.; Temma, N. Mechanical behavior of hydrate-bearing pressure-core sediments visualized under triaxial compression. *Mar. Pet. Geol.* **2015**, *66*, 451–459. [[CrossRef](#)]
101. Zhao, J.; Zheng, J.-N.; Wang, X.; Dong, S.; Yang, M.; Song, Y. Effects of underlying gas on formation and gas production of methane hydrate in muddy low-permeability cores. *Fuel* **2022**, *309*, 122128. [[CrossRef](#)]
102. Priest, J.A.; Hayley, J.L.; Smith, W.E.; Schultheiss, P.; Roberts, J. PCATS triaxial testing: Geomechanical properties of sediments from pressure cores recovered from the Bay of Bengal during expedition NGHP-02. *Mar. Pet. Geol.* **2019**, *108*, 424–438. [[CrossRef](#)]
103. Jang, J.; Dai, S.; Yoneda, J.; Waite, W.F.; Stern, L.A.; Boze, L.-G.; Collett, T.S.; Kumar, P. Pressure core analysis of geomechanical and fluid flow properties of seals associated with gas hydrate-bearing reservoirs in the Krishna-Godavari Basin, offshore India. *Mar. Pet. Geol.* **2019**, *108*, 537–550. [[CrossRef](#)]
104. Wang, B.; Sun, J.; Shen, F.; Li, W.; Zhang, W. Mechanism of wellbore instability in continental shale gas horizontal sections and its water-based drilling fluid countermeasures. *Nat. Gas Ind. B* **2020**, *7*, 680–688. [[CrossRef](#)]
105. Mery, S. Geomechanical wellbore stability analysis for the wells drilled in the shallow sediments of the Mediterranean Sea. *J. Pet. Sci. Eng.* **2020**, *186*, 106714. [[CrossRef](#)]
106. Wu, N.; Li, Y.; Wan, Y.; Sun, J.; Huang, L.; Mao, P. Prospect of marine natural gas hydrate stimulation theory and technology system. *Nat. Gas Ind. B* **2021**, *8*, 173–187. [[CrossRef](#)]
107. Wang, J.-J.; Guo, J.-J.; Bai, J.-P.; Wu, X. Shear strength of sandstone–mudstone particle mixture from direct shear test. *Environ. Earth Sci.* **2018**, *77*, 442. [[CrossRef](#)]
108. Thulasibai, A.S.R.R.; Velayudhan, S.; Pathath, M.; Lekshmpathy, J.; Visvanathan, A. Experimental and Numerical Evaluation of the Parameters Influencing the Shear-Stress Behavior of Interlocking Paver Blocks–Bedding Sand Interface Using Large-Scale Direct Shear Test. *J. Mater. Civ. Eng.* **2021**, *33*, 04021104. [[CrossRef](#)]
109. Liu, Z.; Wei, H.; Peng, L.; Wei, C.; Ning, F. An easy and efficient way to evaluate mechanical properties of gas hydrate-bearing sediments: The direct shear test. *J. Pet. Sci. Eng.* **2017**, *149*, 56–64. [[CrossRef](#)]
110. Santamarina, J.C.; Dai, S.; Terzariol, M.; Jang, J.; Waite, W.F.; Winters, W.J.; Nagao, J.; Yoneda, J.; Konno, Y.; Fujii, T.; et al. Hydro-bio-geomechanical properties of hydrate-bearing sediments from Nankai Trough. *Mar. Pet. Geol.* **2015**, *66*, 434–450. [[CrossRef](#)]
111. Santamarina, J.C.; Dai, S.; Jang, J.; Terzariol, M. Pressure Core Characterization Tools for Hydrate-Bearing Sediments. *Sci. Drill.* **2012**, *14*, 44–48. [[CrossRef](#)]
112. Li, D.; Yin, K.; Glade, T.; Leo, C. Effect of over-consolidation and shear rate on the residual strength of soils of silty sand in the Three Gorges Reservoir. *Sci. Rep.* **2017**, *7*, 5503. [[CrossRef](#)]
113. Swize, T.; Osei-Yeboah, F.; Peterson, M.L.; Boulas, P. Impact of Shear History on Powder Flow Characterization Using a Ring Shear Tester. *J. Pharm. Sci.* **2019**, *108*, 750–754. [[CrossRef](#)]
114. Lian, B.; Wang, X.; Peng, J.; Huang, Q. Shear rate effect on the residual strength characteristics of saturated loess in naturally drained ring shear tests. *Nat. Hazards Earth Syst. Sci.* **2020**, *20*, 2843–2856. [[CrossRef](#)]
115. Kimura, S.; Ito, T.; Noda, S.; Kaneko, H.; Suzuki, K.; Yasuda, H.; Minagawa, H. Water Permeability Evolution With Faulting for Unconsolidated Turbidite Sand in a Gas-Hydrate Reservoir in the Eastern Nankai Trough Area of Japan. *J. Geophys. Res. Solid Earth* **2019**, *124*, 13415–13426. [[CrossRef](#)]
116. Kimura, S.; Kaneko, H.; Ito, T.; Minagawa, H. Investigation of Fault Permeability in Sands with Different Mineral Compositions (Evaluation of Gas Hydrate Reservoir). *Energies* **2015**, *8*, 7202–7223. [[CrossRef](#)]
117. Kimura, S.; Kaneko, H.; Ito, T.; Minagawa, H. The effect of effective normal stress on particle breakage, porosity and permeability of sand: Evaluation of faults around methane hydrate reservoirs. *Tectonophysics* **2014**, *630*, 285–299. [[CrossRef](#)]
118. De Dalal, S.S. Use of cone penetrometer in exploring alluvial Bengal. In Proceedings of the Geoshore International Conference on Offshore and Nearshore Geotechnical Engineering, Panvel, India, 2–3 December 1999; pp. 167–172.
119. Bao, H.; Ye, Z. Estimation of the Pile Foundation Site Considering the Bearing Value of Pile with Static Sounding. *Build. Struct.* **2004**, *34*, 61–62, 65.
120. Jian, W.; Wu, Z.; Liu, H.; Chen, Z.; Zhang, M. Correlation analysis of static sounding parameter of soft soil along coastal area of Southeast Fujian Province. *Rock Soil Mech.* **2005**, *26*, 733–738.
121. Jian, W.; Wu, Z.; Tong, W.; Li, H.; Zhang, M. Consolidation state of soft soil differentiated by static cone sounding. *Chin. J. Rock Mech. Eng.* **2005**, *24*, 2166–2169.
122. Wang, J.; Qin, C.; Luo, X.; Wang, S.; Yang, N. Application prospect of CPT in gas hydrate exploration. *Chin. J. Mar. Geol. Front.* **2019**, *35*, 52–59.
123. Chen, Q.; Li, Y.; Shen, Z.; Wu, N.; Liu, C.; Sun, J. Cone Penetration Test Device and Method for Hydrate-Containing Sediment. CN Patent Application No. CN211401934U, 1 September 2020.
124. Li, Y.; Chen, Q.; Liu, C.; Wu, N.; Sun, J.; Shen, Z.; Zhang, M.; Hu, G. Development of engineering-geological parameters evaluation system for hydrate-bearing sediment and its functional verification. *Chin. J. Mar. Geol. Quat. Geol.* **2020**, *40*, 192–200.